Near-Maximal Mixing of Scalar Gluonium and Quark Mesons: A Gaussian Sum-Rule Analysis

D. Harnett*, R.T. Kleiv†, K. Moats‡, T.G. Steele§

June 19, 2009

Abstract

Gaussian QCD sum-rules are ideally suited to the study of mixed states of gluonium (glueballs) and quark ($q\bar{q}$) mesons because of their capability to resolve widely-separated states of comparable strength. The Gaussian QCD sum-rules (GSRs) for all possible two-point correlation functions of gluonic and non-strange $I = 0$ quark scalar ($J^{PC} = 0^{++}$) currents are calculated and analyzed. For the non-diagonal sum-rule of gluonic and $q\bar{q}$ currents we show that perturbative contributions are chirally-suppressed compared to non-perturbative effects of the quark condensate and instantons, implying that the mixing of quark mesons and gluonium is of non-perturbative origin. The independent predictions of the masses and relative coupling strengths from the non-diagonal and the two diagonal GSRs are remarkably consistent with a scenario of strongly-mixed states with masses of approximately 1 GeV and 1.4 GeV. The mixing is nearly maximal with the heavier mixed state having a slightly larger gluonium content than the lighter state.

1 Introduction

The interpretation of the nature of the lightest scalar mesons is one of the most fascinating problems in hadronic physics. The plethora of scalar ($J^{PC} = 0^{++}$, $I = 0$) states below 2 GeV [1] cannot be described by a simple $q\bar{q}$ nonet, a situation indicative of exotic states such as gluonium (glueballs) or multi-quark ($q\bar{q}q\bar{q}$) states amongst the known scalar mesons. In the case of gluonium states, analyses based on chiral Lagrangians [2, 3] suggest that the $f_0(1500)$ and $f_0(1710)$ are mainly gluonium states with a small gluonium component of the $f_0(980)$ [2]. Similarly, QCD Laplace sum-rules based upon (diagonal) correlation functions of either gluonic or $q\bar{q}$ currents find that admixtures of gluonium and $q\bar{q}$ exist with masses of approximately 1 GeV and 1.6 GeV [4, 5, 6], a conclusion that is also upheld by studies based on Gaussian QCD sum-rules [7, 8, 9]. Phenomenological analyses present a scenario of mixing between a 1 GeV glueball and the $f_0(980)$, $f_0(1500)$ states of a $q\bar{q}$ nonet [10]. Lattice QCD calculations lead to a scalar gluonium state of approximately 1.6 GeV with quenched quarks [11]. However, with dynamical quarks the mixing with $q\bar{q}$ states appears to be very strong, driving the mass of the lightest "flavour-singlet" meson[1] down toward 1 GeV with tentative identification of an excited state on the order of 1.5 GeV [12].

The results of these different approaches suggest a consistent scenario where the mixing of $q\bar{q}$ and gluonium is manifested in the scalar hadronic spectrum as a lighter state on the order of 1 GeV and a heavier state on the order of 1.5 GeV. From both the QCD sum-rule and lattice perspectives, this implies that states exist which couple to both gluonic currents and to quark currents, and hence the non-diagonal correlation function between $q\bar{q}$ and gluonic currents must be non-trivial. Surprisingly, the study of such non-diagonal correlation functions has been largely ignored apart from the use of low-energy theorems [13]; to our knowledge Ref. [14] is the only study of non-diagonal gluonic-$q\bar{q}$ correlation functions and its detailed analysis is limited to the pseudoscalar case. Analysis of the non-diagonal correlation functions is thus essential for a complete understanding of the scalar gluonium-$q\bar{q}$ system.

Gaussian sum-rules have been shown to be sensitive to the hadronic spectral functions over a broad energy range, and analysis techniques have been developed to exploit this dependence to determine how resonance strength is distributed in the spectral function [7, 8, 9]. Thus Gaussian sum-rules are well-suited to situations such as $q\bar{q}$-gluonium mixing where multiple hadronic states could contribute to a correlation function.

*Department of Physics, University of the Fraser Valley, Abbotsford, BC, V2S 7M8, Canada
†Department of Physics and Engineering Physics, University of Saskatchewan, Saskatoon, SK, S7N 5E2, Canada
‡Department of Physics, Carleton University, Ottawa, ON, K1S 5B6, Canada
§Department of Physics and Engineering Physics, University of Saskatchewan, Saskatoon, SK, S7N 5E2, Canada

[1] In Ref. [12] it is noted that the distinction between gluonium and $q\bar{q}$ mesons is obscured; one has gluonic and $q\bar{q}$ operators which couple to flavour-singlet mesons.

The purpose of this paper is to demonstrate that all possible Gaussian sum-rules for two-point correlation functions amongst gluonic and $q\bar{q}$ currents (*i.e.* diagonal gluonic, diagonal $q\bar{q}$, non-diagonal gluonic-$q\bar{q}$) lead to a consistent scenario for strong (near-maximal) mixing of gluonium and $q\bar{q}$ scalar mesons. The formulation and analysis of Gaussian sum-rules is reviewed in Section 2, and previous results for the diagonal gluonic and $q\bar{q}$ Gaussian sum-rules are presented. In Section 3 the leading-order perturbative, QCD condensate, and instanton contributions to the non-diagonal correlation function of $q\bar{q}$ and gluonic currents are calculated along with the associated Gaussian QCD sum-rule. The analysis of the Gaussian sum-rules and the pattern of state coupling mixing is then presented in Section 4.

2 Review of Gaussian Sum-Rules

The simplest Gaussian QCD sum-rule (GSR) has the form [15]

$$G_0\left(\hat{s},\tau\right) = \frac{1}{\sqrt{4\pi\tau}} \int\limits_{t_0}^{\infty} \exp\left[\frac{-\left(t-\hat{s}\right)^2}{4\tau}\right] \frac{1}{\pi}\rho(t)\,\mathrm{d}\,t \quad , \quad \tau > 0 \tag{1}$$

and relates the QCD prediction $G_0\left(\hat{s},\tau\right)$ to an integral of its associated hadronic spectral function $\rho(t)$. The smearing of the spectral function by the Gaussian kernel peaked at $t = \hat{s}$ through the (approximate) region $\hat{s} - 2\sqrt{\tau} \leq t \leq \hat{s} + 2\sqrt{\tau}$ provides a clear conceptual implementation of quark-hadron duality. The width of this duality interval is constrained by QCD since renormalization-group improvement of the QCD (left-hand) side of (1) results in identifying the renormalization scale ν through $\nu^2 = \sqrt{\tau}$ [8, 15]; therefore it is not possible to achieve the formal $\tau \to 0$ limit where complete knowledge of the spectral function could be obtained through

$$\lim_{\tau\to 0} G_0\left(\hat{s},\tau\right) = \frac{1}{\pi}\rho\left(\hat{s}\right) \quad , \quad \hat{s} > t_0 \quad . \tag{2}$$

The variable $\hat{s}$ in (1), on the other hand, is unconstrained by QCD, and so the $\hat{s}$ dependence of $G_0\left(\hat{s},\tau\right)$ can be used to probe the behaviour of the smeared spectral function, and hence the essential features of $\rho(t)$ can be extracted.

An interesting feature of the GSR (1) is its ability to study excited and ground states with similar sensitivity. For example, as $\hat{s}$ passes through t values corresponding to resonance peaks, the Gaussian kernel reaches its maximum value. Thus any features of the spectral function strong enough to be isolated from the continuum will be revealed through the GSR. In this regard, GSRs should be contrasted with Laplace sum-rules

$$R\left(\Delta^2\right) = \frac{1}{\pi} \int\limits_{t_0}^{\infty} \exp\left(-\frac{t}{\Delta^2}\right)\rho(t)\,\mathrm{d}\,t \quad , \tag{3}$$

which exponentially suppress excited states in comparison to the ground state.

Gaussian sum-rules are based on QCD correlation functions $\Pi\left(Q^2\right)$ of renormalized composite operators $J_1(x)$ and $J_2(x)$[2]

$$\Pi\left(Q^2\right) = \mathrm{i}\int \mathrm{d}^4x\; \mathrm{e}^{\mathrm{i}q\cdot x}\,\langle 0|T\left[J_1(x)J_2(0)\right]|0\rangle \quad , \quad Q^2 \equiv -q^2 \; . \tag{4}$$

By allowing the possibility that $J_1 \neq J_2$, our formulation encompasses both diagonal ($J_1 = J_2$) and non-diagonal correlation functions. The correlation function (4) will satisfy dispersion relations appropriate to the asymptotic form of the correlator in question. For example, the diagonal scalar gluonic correlation function $\Pi\left(Q^2\right)$ satisfies the following dispersion relation with three subtraction constants

$$\Pi\left(Q^2\right) - \Pi(0) - Q^2\Pi'(0) - \frac{1}{2}Q^4\Pi''(0) = -\frac{Q^6}{\pi} \int\limits_{t_0}^{\infty} \frac{\rho(t)}{t^3\left(t+Q^2\right)}\,\mathrm{d}\,t \quad . \tag{5}$$

In general, the quantity $\rho(t)$ is the spectral function appropriate to the quantum numbers of the given currents, and it should be noted that in certain situations (such as the scalar gluonic correlation function) the subtraction constant

[2]The configuration-space correlation function in (4) as used in lattice QCD will contain an exponential suppression of excited states similar to that occurring for Laplace sum-rules.

$\Pi(0)$ is determined by a low-energy theorem [13]. Undetermined dispersion-relation constants and field-theoretical divergences are eliminated upon constructing the GSR [7][3]

$$G_k(\hat{s},\tau) \equiv \sqrt{\frac{\tau}{\pi}}\mathcal{B}\left\{\frac{(\hat{s}+\mathrm{i}\Delta)^k\Pi(-\hat{s}-\mathrm{i}\Delta)-(\hat{s}-\mathrm{i}\Delta)^k\Pi(-\hat{s}+\mathrm{i}\Delta)}{\mathrm{i}\Delta}\right\} \tag{6}$$

where $k=-1,0,1,\ldots$ and where the Borel transform $\mathcal{B}$ is defined by

$$\mathcal{B} \equiv \lim_{\substack{N,\Delta^2\to\infty \\ \Delta^2/N\equiv 4\tau}} \frac{(-\Delta^2)^N}{\Gamma(N)}\left(\frac{\mathrm{d}}{\mathrm{d}\Delta^2}\right)^N \quad . \tag{7}$$

The dispersion relation (5) in conjunction with definition (6) together yield the following family of GSRs

$$G_k(\hat{s},\tau)+\delta_{k\,-1}\frac{1}{\sqrt{4\pi\tau}}\exp\left(\frac{-\hat{s}^2}{4\tau}\right)\Pi(0)=\frac{1}{\sqrt{4\pi\tau}}\int_{t_0}^{\infty}t^k\exp\left[\frac{-(\hat{s}-t)^2}{4\tau}\right]\frac{1}{\pi}\rho(t)\,\mathrm{d}\,t\ , \tag{8}$$

where the identity

$$\mathcal{B}\left[\frac{1}{\Delta^2+a}\right]=\frac{1}{4\tau}\exp\left(\frac{-a}{4\tau}\right) \quad , \quad n=0,1,2,\ldots \tag{9}$$

has been used to simplify the phenomenological (right-hand) side of (8) as well as the term on the QCD side proportional to $\Pi(0)$. Clearly the $k=-1$ sum-rule can only be defined in cases where there exists an appropriate low-energy theorem because $\Pi(0)$ is present in (8) when $k=-1$. Calculation of $G_k(\hat{s},\tau)$ is achieved through an identity relating (7) to the inverse Laplace transform [15]

$$\mathcal{B}[f(\Delta^2)]=\frac{1}{4\tau}\mathcal{L}^{-1}[f(\Delta^2)] \tag{10}$$

where, in our notation,

$$\mathcal{L}^{-1}[f(\Delta^2)]=\frac{1}{2\pi\mathrm{i}}\int_{a-\mathrm{i}\infty}^{a+\mathrm{i}\infty}f(\Delta^2)\exp\left(\frac{\Delta^2}{4\tau}\right)\mathrm{d}\,\Delta^2 \tag{11}$$

with a chosen such that all singularities of f lie to the left of a in the complex Δ^2-plane (see [7] for further details).

Next, we impose a fairly general resonance(s) plus continuum model

$$\rho(t)=\rho^{\mathrm{had}}(t)+\theta\,(t-s_0)\,\mathrm{Im}\Pi^{\mathrm{QCD}}(t) \tag{12}$$

where s_0 represents the onset of the QCD continuum. The continuum contribution of (12) to the right-hand side of (8) is

$$G_k^{\mathrm{cont}}(\hat{s},\tau,s_0)=\frac{1}{\sqrt{4\pi\tau}}\int_{s_0}^{\infty}t^k\exp\left[\frac{-(\hat{s}-t)^2}{4\tau}\right]\frac{1}{\pi}\mathrm{Im}\Pi^{\mathrm{QCD}}(t)\,\mathrm{d}\,t \quad , \tag{13}$$

and is combined with $G_k\,(\hat{s},\tau)$ to obtain the total QCD contribution

$$G_k^{\mathrm{QCD}}\,(\hat{s},\tau,s_0)\equiv G_k\,(\hat{s},\tau)-G_k^{\mathrm{cont}}\,(\hat{s},\tau,s_0) \quad , \tag{14}$$

resulting in the final relation between the QCD and hadronic sides of the GSRs

$$G_k^{\mathrm{QCD}}\,(\hat{s},\tau,s_0)+\delta_{k\,-1}\frac{1}{\sqrt{4\pi\tau}}\exp\left(\frac{-\hat{s}^2}{4\tau}\right)\Pi(0)=\frac{1}{\sqrt{4\pi\tau}}\int_{t_0}^{\infty}t^k\exp\left[\frac{-(\hat{s}-t)^2}{4\tau}\right]\frac{1}{\pi}\rho^{\mathrm{had}}(t)\,\mathrm{d}\,t \quad . \tag{15}$$

Original studies involving the GSRs exploited the diffusion equation

$$\frac{\partial^2 G_0\,(\hat{s},\tau)}{\partial\hat{s}^2}=\frac{\partial G_0\,(\hat{s},\tau)}{\partial\tau} \tag{16}$$

[3]This definition is a natural generalization of that given in [15]. To recover the original GSR, we simply let $k=0$ in (6).

which follows from (8) for $k=0$. In particular, when $\rho^{\rm had}(t)$ [see (12)] is evolved through the diffusion equation (16), it only reproduces the QCD prediction at large energies (τ large) if the resonance and continuum contributions are balanced through the $k=0$ member of the finite-energy sum-rule family [15]

$$F_k\left(s_0\right)=\frac{1}{\pi}\int\limits_{t_0}^{s_0}t^k\rho^{\rm had}(t)\,{\rm d}\,t \quad . \tag{17}$$

An additional connection between the finite-energy sum-rules (17) and the GSRs can be found by integrating both sides of (15) with respect to $\hat{s}$ to obtain

$$\int\limits_{-\infty}^{\infty}G_k^{\rm QCD}(\hat{s},\tau,s_0)\,{\rm d}\,\hat{s}+\delta_{k\,-1}\Pi(0)=\frac{1}{\pi}\int\limits_{t_0}^{\infty}t^k\rho^{\rm had}(t)\,{\rm d}\,t \quad , \tag{18}$$

indicating that the finite-energy sum-rules (17) are related to the normalization of the GSRs. Thus the information independent of the finite-energy sum-rule constraint following from the diffusion equation analysis [15] is contained in the *normalized* Gaussian sum-rules (NGSRs) [8]

$$N_k^{\rm QCD}(\hat{s},\tau,s_0)=\frac{G_k^{\rm QCD}(\hat{s},\tau,s_0)+\delta_{k\,-1}\frac{1}{\sqrt{4\pi\tau}}\exp\left(\frac{-\hat{s}^2}{4\tau}\right)\Pi(0)}{M_k^{\rm QCD}(\tau,s_0)+\delta_{k\,-1}\Pi(0)} \tag{19}$$

$$M_k^{\rm QCD}(\tau,s_0)=\int\limits_{-\infty}^{\infty}G_k^{\rm QCD}(\hat{s},\tau,s_0)\,{\rm d}\,\hat{s} \quad , \quad n=0,1,2,\ldots \quad , \tag{20}$$

which are related to the hadronic spectral function via

$$N_k^{\rm QCD}(\hat{s},\tau,s_0)=\frac{\frac{1}{\sqrt{4\pi\tau}}\int_{t_0}^{\infty}t^k\exp\left[\frac{-(\hat{s}-t)^2}{4\tau}\right]\rho^{\rm had}(t)\,{\rm d}\,t}{\int_{t_0}^{\infty}t^k\rho^{\rm had}(t)\,{\rm d}\,t} \quad . \tag{21}$$

For diagonal correlation functions the spectral function obeys a positivity constraint so the NGSR must exist. For non-diagonal correlators the possibility of state mixing implies that $\rho^{\rm had}(t)$ could change sign, so it is possible that either $M_k^{\rm QCD}(\tau,s_0)$ or that the denominator on the right-hand side of (21) could be zero. In such situations, the GSR (15) would have to be analyzed instead of the NGSR (21).

We now consider the currents that will be used to probe the gluonic and $q\bar{q}$ aspects of the hadronic states. Refs. [4, 16] argue quite eloquently that the mixing of $q\bar{q}$ mesons and gluonium is unavoidable because of the trace anomaly for the energy-momentum tensor $T_{\mu\nu}$ [17]

$$T_\mu^\mu=\frac{1}{4}\beta(\alpha)G_{\mu\nu}^aG^{a\,\mu\nu}+\left[1+\gamma(\alpha)\right]\sum_f m_i\bar{\psi}_f\psi_f \tag{22}$$

where

$$2\pi\alpha\beta\left(\alpha\right)=\nu^2\frac{\rm d}{{\rm d}\nu^2}\left(\frac{\alpha}{\pi}\right)=-\beta_0\left(\frac{\alpha}{\pi}\right)^2-\beta_1\left(\frac{\alpha}{\pi}\right)^3+\ldots \tag{23}$$

$$\beta_0=\frac{11}{4}-\frac{1}{6}n_f \quad , \quad \beta_1=\frac{51}{8}-\frac{19}{24}n_f \tag{24}$$

$$-2m\gamma(\alpha)=\nu^2\frac{\rm dm}{{\rm d}\nu^2}\ . \tag{25}$$

In fact, (22) contains two multiplicatively-renormalizable (renormalization-group invariant) composite operators $m\bar{\psi}\psi$ and $\beta G^2+4\gamma m\bar{\psi}\psi$, so from a field theoretical perspective these two operators would be suitable choices for currents. However, with this choice the gluonic or $q\bar{q}$ nature of states coupled to the current $\beta G^2+4\gamma m\bar{\psi}\psi$ is obscured. Instead, we follow [14] and choose the renormalized currents

$$J_g(x)=\alpha G_R^2=\alpha\left(1+\frac{\beta_0}{\epsilon}\frac{\alpha}{\pi}\right)G_B^2-4\alpha\frac{\alpha}{\pi}\frac{1}{\epsilon}\left[m_u\overline{u}(x)u(x)+m_d\overline{d}(x)d(x)\right]_B+\ldots \tag{26}$$

$$J_q(x)=m_q\left[\overline{u}(x)u(x)+\overline{d}(x)d(x)\right]\ ,\ m_q=\left(m_u+m_d\right)/2. \tag{27}$$

where the notation R refers to the renormalized composite operator and the B denotes an expansion in terms of bare quantities and our convention for dimensional regularization uses $D = 4 + 2\epsilon$ spacetime dimensions. Of course the form of the renormalized operator (26) necessarily underlies the renormalization-group invariance of the trace anomaly (22) (see *e.g.* [18]). However, the advantage of the current J_g is that its tree-level expansion is purely gluonic allowing a qualitative separation of gluonic and $q\bar{q}$ degrees of freedom. The current J_q has isospin $I = 0$ and is renormalization-group invariant.

The diagonal correlation function for the gluonic currents J_g is defined by

$$\Pi_{gg}\left(Q^2\right) = \mathrm{i}\int \mathrm{d}^4x\, \mathrm{e}^{\mathrm{i}q\cdot x}\,\langle 0|T\left[J_g(x)J_g(0)\right]|0\rangle \quad , \quad Q^2 \equiv -q^2 \tag{28}$$

while the diagonal correlation function of the $I = 0$ (non-strange) quark currents J_q is

$$\Pi_{qq}\left(Q^2\right) = \mathrm{i}\int \mathrm{d}^4x\, \mathrm{e}^{\mathrm{i}q\cdot x}\,\langle 0|T\left[J_q(x)J_q(0)\right]|0\rangle \quad , \quad Q^2 \equiv -q^2. \tag{29}$$

Although both the gluonic and ($I = 0$) quark diagonal correlation functions are probes of scalar hadronic states, those states which have a more significant overlap with the gluonic current should predominate in (28), while those states which are dominantly of a quark ($q\bar{q}$) nature should be more significant in (29). A mixed state with substantial gluonic and quark components (*i.e.* a state that overlaps with both the gluonic and quark currents) should self-consistently appear in an analysis of both correlation functions. In particular, prediction of mass-degenerate states from the QCD sum-rule analysis associated with these two correlation functions is indicative of a mixed state.

In the scalar gluonic channel, the low-energy theorem (LET) [13]

$$\Pi_{gg}(0) \equiv \lim_{Q^2\to 0}\Pi_{gg}(Q^2) = \frac{8\pi}{\beta_0}\langle\alpha G^2\rangle \tag{30}$$

allows construction of the $k = -1$ GSR. The significance of instanton contributions in the overall consistency of the LET-sensitive $k = -1$ sum-rule and the LET-insensitive $k \geq 0$ sum-rules was first demonstrated for Laplace sum-rules [19, 20]. A similar consistency is observed for the Gaussian sum-rules, but theoretical uncertainties are better controlled in the $k \geq 0$ GSR [7], and hence this paper will focus on the $k = 0$ GSRs for the diagonal gluonic and quark channels.

The QCD correlation functions (28) and (29) contain perturbative, condensate, and instanton contributions. For the diagonal scalar gluonic case, the QCD prediction for the $k = 0$ GSR to leading order in the quark mass is [7][4]

$$\begin{aligned} G_0^{(gg)}(\hat{s},\tau,s_0) = &-\frac{1}{\sqrt{4\pi\tau}}\int_0^{s_0} t^2\exp\left[\frac{-(\hat{s}-t)^2}{4\tau}\right]\left[(a_0-\pi^2a_2)+2a_1\log\left(\frac{t}{\nu^2}\right)+3a_2\log^2\left(\frac{t}{\nu^2}\right)\right]\mathrm{d}\,t \\ &-\frac{1}{\sqrt{4\pi\tau}}b_1\langle\alpha G^2\rangle\int_0^{s_0}\exp\left[\frac{-(\hat{s}-t)^2}{4\tau}\right]\mathrm{d}\,t+\frac{1}{\sqrt{4\pi\tau}}\exp\left(\frac{-\hat{s}^2}{4\tau}\right)\left[c_0\,\langle\mathcal{O}_6\rangle-\frac{d_0\hat{s}}{2\tau}\,\langle\mathcal{O}_8\rangle\right] \\ &-\frac{16\pi^3}{\sqrt{4\pi\tau}}n_c\rho^4\int_0^{s_0} t^2\exp\left[\frac{-(\hat{s}-t)^2}{4\tau}\right]J_2\left(\rho\sqrt{t}\right)Y_2\left(\rho\sqrt{t}\right)\mathrm{d}\,t \quad . \end{aligned} \tag{31}$$

The perturbative coefficients in (31) are given by

$$\begin{aligned} a_0 &= -2\left(\frac{\alpha}{\pi}\right)^2\left[1+\frac{659}{36}\frac{\alpha}{\pi}+247.480\left(\frac{\alpha}{\pi}\right)^2\right] \\ a_1 = 2\left(\frac{\alpha}{\pi}\right)^3&\left[\frac{9}{4}+65.781\frac{\alpha}{\pi}\right] \quad , \quad a_2 = -10.1250\left(\frac{\alpha}{\pi}\right)^4 \ , \end{aligned} \tag{32}$$

as obtained from the three-loop $\overline{\mathrm{MS}}$ calculation of the correlation function in the chiral limit of $n_f = 3$ flavours [21]. The condensate contributions in (31) involve next-to-leading order [22] contributions from the dimension four gluon

[4] To leading chiral order the GSR is identical for the current (26) or the trace-anomaly version $\beta G^2 + 4\gamma m\bar{q}q$.

condensate $\langle \alpha G^2 \rangle$ and leading order [23] contributions from gluonic condensates of dimension six and eight

$$\langle \mathcal{O}_6 \rangle = \left\langle g f_{abc} G^a_{\mu\nu} G^b_{\nu\rho} G^c_{\rho\mu} \right\rangle \tag{33}$$

$$\langle \mathcal{O}_8 \rangle = 14 \left\langle \left(\alpha f_{abc} G^a_{\mu\rho} G^b_{\nu\rho} \right)^2 \right\rangle - \left\langle \left(\alpha f_{abc} G^a_{\mu\nu} G^b_{\rho\lambda} \right)^2 \right\rangle \tag{34}$$

$$\begin{aligned} b_0 = 4\pi \frac{\alpha}{\pi} \left[1 + \frac{175}{36} \frac{\alpha}{\pi} \right] \quad , \quad b_1 = -9\pi \left(\frac{\alpha}{\pi} \right)^2 \quad , \\ c_0 = 8\pi^2 \left(\frac{\alpha}{\pi} \right)^2 \quad , \quad d_0 = 8\pi^2 \frac{\alpha}{\pi} \quad . \end{aligned} \tag{35}$$

The remaining term in the GSR (31) represents instanton contributions obtained from single instanton and anti-instanton [24] (*i.e.,* that multi-instanton effects are negligible [25]) contributions to the scalar gluonic correlator [19, 20, 23, 26] within the liquid instanton model [19] parameterized by the instanton size ρ and the instanton density n_c. The quantities J_2 and Y_2 are Bessel functions in the notation of [27].

As a result of renormalization-group scaling of the GSRs [8, 15], the coupling in the perturbative and condensate coefficients [(32) and (35)] is implicitly the running coupling at the scale $\nu^2 = \sqrt{\tau}$ for $n_f = 3$ in the $\overline{\rm MS}$ scheme

$$\begin{aligned} \frac{\alpha(\nu^2)}{\pi} = \frac{1}{\beta_0 L} - \frac{\bar{\beta}_1 \log L}{(\beta_0 L)^2} + \frac{1}{(\beta_0 L)^3} \left[\bar{\beta}_1^2 \left(\log^2 L - \log L - 1 \right) + \bar{\beta}_2 \right] \\ L = \log \left(\frac{\nu^2}{\Lambda^2} \right) \quad , \quad \bar{\beta}_i = \frac{\beta_i}{\beta_0} \quad , \quad \beta_0 = \frac{9}{4} \quad , \quad \beta_1 = 4 \quad , \quad \beta_2 = \frac{3863}{384} \end{aligned} \tag{36}$$

with $\Lambda_{\overline{MS}} \approx 300\,\text{MeV}$ for three active flavours, consistent with current determinations of $\alpha(M_\tau)$ [1].

Analogous to the scalar gluonic case, the QCD prediction of $k = 0$ diagonal GSR for the $I = 0$ scalar quark currents to leading order in the quark mass is [8]

$$\begin{aligned} G_0^{(qq)}(\hat{s}, \tau, s_0) = & \frac{1}{\sqrt{4\pi\tau}} \frac{3m_q^2}{16\pi^2} \int_0^{s_0} \exp\left[-\frac{(t-\hat{s})^2}{4\tau} \right] \left[t \left(1 + \frac{17}{3} \frac{\alpha}{\pi} \right) - 2\frac{\alpha}{\pi} t \log\left(\frac{t}{\nu^2} \right) \right] \, \mathrm{d}\, t \\ & + m_q^2 \exp\left(-\frac{\hat{s}^2}{4\tau} \right) \left[\frac{1}{2\sqrt{\pi\tau}} \langle C_4^s \mathcal{O}_4^s \rangle - \frac{\hat{s}}{4\tau\sqrt{\pi\tau}} \langle C_6^s \mathcal{O}_6^s \rangle \right] \\ & - \frac{3m_q^2}{8\pi} \frac{1}{\sqrt{4\pi\tau}} \int_0^{s_0} t \exp\left[-\frac{(t-\hat{s})^2}{4\tau} \right] J_1\left(\rho\sqrt{t} \right) Y_1\left(\rho\sqrt{t} \right) \, \mathrm{d}\, t \quad . \end{aligned} \tag{37}$$

Again, renormalization-group improvement implies that both m_q and α are implicitly running quantities at the scale $\nu^2 = \sqrt{\tau}$ as given by (36) and the (two-loop, $n_f = 3$, $\overline{\rm MS}$) expression

$$m_q\left(\nu^2\right) = \frac{\hat{m}_q}{\left(\frac{1}{2}L\right)^{\frac{4}{9}}} \left(1 + \frac{290}{729} \frac{1}{L} - \frac{256}{729} \frac{\log L}{L} \right) \quad , \quad L = \log\left(\frac{\nu^2}{\Lambda^2} \right) \quad , \tag{38}$$

where $\hat{m}_q$ is the renormalization-group invariant quark mass parameter. The perturbative contributions in (37) are the $n_f = 3$ two-loop results obtained from [28], and the instanton expressions are obtained from [29]. The condensate contributions are leading-order results obtained from [29], and are defined by the quantities

$$\langle C_4^s \mathcal{O}_4^s \rangle = \frac{3}{2} \langle m_q \overline{q} q \rangle + \frac{1}{16\pi} \langle \alpha_s G^2 \rangle \ , \ \langle \overline{q} q \rangle \equiv \frac{1}{2} \langle \bar{u}u + \bar{d}d \rangle \tag{39}$$

and

$$\langle C_6^s \mathcal{O}_6^s \rangle = \pi\alpha_s \left[\frac{1}{4} \left\langle \left(\bar{u}\sigma_{\mu\nu}\lambda^a u - \bar{d}\sigma_{\mu\nu}\lambda^a d \right)^2 \right\rangle + \frac{1}{6} \left\langle \left(\bar{u}\gamma_\mu\lambda^a u + \bar{d}\gamma_\mu\lambda^a d \right) \sum_{u,d,s} \bar{\psi}\gamma^\mu\lambda^a\psi \right\rangle \right] \quad . \tag{40}$$

The vacuum saturation hypothesis [29] in the $SU(2)$ limit $\langle \bar{u}u \rangle = \langle \bar{d}d \rangle \equiv \langle \bar{q}q \rangle$ provides a reference value for $\langle \mathcal{O}_6^s \rangle$

$$\langle C_6^s \mathcal{O}_6^s \rangle = -f_{vs} \frac{88}{27} \alpha_s \langle (\bar{q}q)^2 \rangle = -f_{vs} 1.8 \times 10^{-4} \text{GeV}^6 \quad , \tag{41}$$

where the quantity f_{vs} parameterizes deviations from vacuum saturation where $f_{vs} = 1$.

The GSRs (31) and (37) exhibit some interesting qualitative features. For example, the condensate contributions decay exponentially with the Gaussian peak-position $\hat{s}$, emphasizing that these contributions have a low-energy origin.

3 Non-Diagonal Correlation Function and GSR of $q\bar{q}$ and Gluonic Currents

The non-diagonal correlation function for quark and gluonic currents is defined by

$$\Pi_{gq}\left(Q^2\right) = \mathrm{i}\int \mathrm{d}^4x\, \mathrm{e}^{\mathrm{i}q\cdot x}\left\langle 0\right|T\left[J_g(x)J_q(0)\right]\left|0\right\rangle \quad , \quad Q^2 \equiv -q^2 \ . \tag{42}$$

As with the diagonal correlators, the non-diagonal correlation function contains perturbative, QCD condensate, and instanton contributions.

The leading order perturbative diagrams that contribute to $\Pi_{gq}\left(Q^2\right)$ are given in Figure 1. The first diagram is a two-loop calculation and corresponds to the (bare) gluonic term in (26) while the second is a one-loop calculation corresponding to the (bare) quark term arising from composite-operator renormalization. However, one can see that both diagrams lead to the same order in α.[5] Both diagrams also have the same $\mathcal{O}\left(m_q^2\right)$ leading chiral behaviour; the first diagram results in an $\mathcal{O}\left(m_q\right)$ chiral suppression factor from the quark loop.

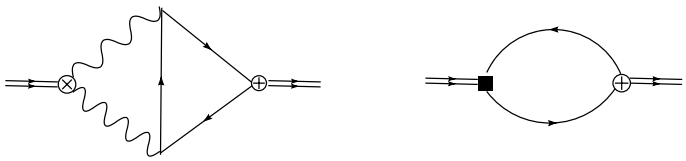

Figure 1: Leading order perturbative diagrams for the non-diagonal correlation function. The symbol $\otimes$ denotes the bare current αG_B^2 within J_g and $\oplus$ denotes the bare current J_q. In the second diagram, the solid square represents the $q\bar{q}$ term arising in the renormalization of J_g. The Feynman diagrams were drawn with JaxoDraw [30].

The two-loop diagram in Figure 1 can be expressed in terms of the fundamental two-loop integrals [31][6]

$$I_2 = \int \frac{d^Dk_1}{(2\pi)^D}\frac{d^Dk_2}{(2\pi)^D}\frac{1}{k_2^2\left(k_1-k_2\right)^2\left(q-k_1\right)^2} = -\frac{1}{(4\pi)^4}q^2\left(-\frac{q^2}{4\pi\nu^2}\right)^{2\epsilon}\frac{\Gamma^3(1+\epsilon)\Gamma(-1-2\epsilon)}{\Gamma(3+3\epsilon)} \tag{43}$$

$$I_3 = \left[\int \frac{d^Dk_1}{(2\pi)^D}\frac{1}{k_1^2\left(q-k_1\right)^2}\right]^2 = -\frac{1}{(4\pi)^4}\left(-\frac{q^2}{4\pi\nu^2}\right)^{2\epsilon}\left[\frac{\Gamma^2(1+\epsilon)\Gamma(-\epsilon)}{\Gamma(2+2\epsilon)}\right]^2 \tag{44}$$

$$I_4 = \int \frac{d^Dk_1}{(2\pi)^D}\frac{d^Dk_2}{(2\pi)^D}\frac{1}{k_1^2\left(q-k_2\right)^2\left(k_1-k_2\right)^2\left(q-k_1\right)^2} = -\frac{1}{(4\pi)^4}\left(-\frac{q^2}{4\pi\nu^2}\right)^{2\epsilon}\frac{\Gamma(-\epsilon)\Gamma(-2\epsilon)\Gamma^3(1+\epsilon)\Gamma(1+2\epsilon)}{\Gamma(1-\epsilon)\Gamma(2+2\epsilon)\Gamma(2+3\epsilon)} \tag{45}$$

$$\begin{aligned} I_5 &= \int \frac{d^Dk_1}{(2\pi)^D}\frac{d^Dk_2}{(2\pi)^D}\frac{k_1^2}{k_2^2\left(q-k_2\right)^2\left(k_1-k_2\right)^2\left(q-k_1\right)^2} \\ &= -\frac{1}{(4\pi)^4}\left(-\frac{q^2}{4\pi\nu^2}\right)^{2\epsilon}q^2\left[\frac{\Gamma(-\epsilon)\Gamma(-2\epsilon)\Gamma^3(1+\epsilon)\Gamma(1+2\epsilon)}{\Gamma(1-\epsilon)\Gamma(2+2\epsilon)\Gamma(2+3\epsilon)} - \frac{2\Gamma(2+\epsilon)\Gamma^2(1+\epsilon)\Gamma(-\epsilon)\Gamma(2+2\epsilon)\Gamma(-2\epsilon)}{\Gamma(3+2\epsilon)\Gamma(1-\epsilon)\Gamma(3+3\epsilon)}\right] \end{aligned} \tag{46}$$

$$\begin{aligned} I_6 &= \int \frac{d^Dk_1}{(2\pi)^D}\frac{d^Dk_2}{(2\pi)^D}\frac{1}{k_1^2k_2^2\left(q-k_2\right)^2\left(k_1-k_2\right)^2\left(q-k_1\right)^2} \\ &= -\frac{1}{q^2(4\pi)^4}\left(-\frac{p^2}{4\pi\nu^2}\right)^{2\epsilon}q^2\frac{\Gamma(-1-2\epsilon)\Gamma^2(\epsilon)\Gamma(1+\epsilon)\Gamma(-2\epsilon)}{\Gamma(1+3\epsilon)}\left[\frac{\Gamma(1+3\epsilon)}{\Gamma(\epsilon)} - \frac{\Gamma(1-\epsilon)}{\Gamma(-3\epsilon)} + \frac{2}{\Gamma(-2\epsilon)}\right] \end{aligned} \tag{47}$$

where we have converted the dimensional regularization conventions in [31] to $D = 4+2\epsilon$. The integral I_6 is strictly not necessary since it is finite, but we provide it for completeness. At leading chiral order, the contribution of the two-loop perturbative diagram to Π_{gq} is

$$\begin{aligned} \Pi_{gq}\left(p^2\right) &= 128\pi\alpha^2m^2\left[-8I_2 + (8-2D)p^2I_3 + (4D-8)p^2I_4 + (4-2D)I_5 + (2-D)p^4I_6\right] \\ &= \alpha^2m^2\frac{3Q^2L}{\pi^3}\frac{1}{\epsilon} + \alpha^2m^2\frac{3Q^2L}{\pi^3}\left[L + 2\gamma - \frac{35}{6}\right] + \text{log independent terms} \ , \ L = \log\left(Q^2/4\pi\nu^2\right) \ . \end{aligned} \tag{48}$$

[5] Strange (and heavier) quarks originating from composite operator renormalization in (26) will be suppressed by a factor of α^2.

[6] Note that the integral I_6 does not appear in the the classification of Ref. [31]; it has been included here for completeness.

The non-logarithmic terms in (48) can be ignored since they correspond to dispersion relation substraction constants which are eliminated when forming the GSR.

The L/ϵ term in (48) is problematic since it cannot be renormalized away or absorbed into a dispersion-relation subtraction constant. However, the leading chiral order contribution of the one-loop diagram of Figure 1 to Π_{gq} is

$$-i\frac{48\alpha^2 m^2 Q^2}{\epsilon\pi}J_1 \ , \tag{49}$$

where we have introduced the following notation for one-loop integrals:

$$J_1 = \int \frac{d^D k}{(2\pi)^D}\frac{1}{k^2(q-k)^2} \ , \tag{50}$$

$$J_2 = \int \frac{d^D k}{(2\pi)^D}\frac{1}{k^2(q-k)^4} = \int \frac{d^D k}{(2\pi)^D}\frac{1}{k^4(q-k)^2} \ , \tag{51}$$

$$J_3 = \int \frac{d^D k}{(2\pi)^D}\frac{1}{k^4(q-k)^4} \ . \tag{52}$$

Thus the contribution of the one-loop "renormalization" diagram to Π_{gq} is

$$-\alpha^2 m^2 \frac{3Q^2 L}{\pi^3}\frac{1}{\epsilon} + \text{log independent terms} \ , \tag{53}$$

which cancels the problematic L/ϵ term from the two-loop diagram. Thus the leading-order perturbative contributions to the non-diagonal correlation function are

$$\Pi_{gq}^{pert}\left(Q^2\right) = m^2 Q^2\left[A_0 L + A_1 L^2\right] \tag{54}$$

$$A_0 = \frac{3}{\pi}\left(\frac{\alpha}{\pi}\right)^2\left(2\gamma - \frac{35}{6}\right) \ , \ A_1 = \frac{3}{\pi}\left(\frac{\alpha}{\pi}\right)^2 \ . \tag{55}$$

This result disagrees with that presented in Ref. [14], although the overall chiral and logarithmic dependence is qualitatively similar. We have checked our calculational methodology by verifying the pseudoscalar results in [14] and believe that (55) is correct.[7]

The quark condensate contributions to the non-diagonal correlator are easily calculated to leading chiral order using any of the equivalent methods for evaluating operator-product expansion coefficients [32]. As in the perturbative case, in principle there are the two classes of diagrams shown in Figure 2. However, the result of the first set of diagrams of Fig. 2 is

$$32i\frac{\pi}{3}\alpha^2 m_q\langle\bar{q}q\rangle\left[(-2D-4)J_1 + (2D-4)q^2 J_2 + (2-D)q^4 J_3\right] = -\frac{8}{\pi}\alpha^2 m_q\langle\bar{q}q\rangle\log\left(\frac{Q^2}{\nu^2}\right) \tag{56}$$

where logarithm-independent terms have been ignored as they correspond to dispersion relation substraction constants which are eliminated when forming the GSR. The "renormalization-induced" diagram of Fig. 2 is chirally-suppressed relative to (56) so it represents subleading effects.

It is more difficult to calculate the gluon condensate contributions, which may explain why the non-diagonal correlators have not previously been the subject of detailed study. The diagrams that could lead to the gluon condensate contributions are shown in Figure 3. However, the "renormalization-induced" diagrams are higher-order in α and hence are subleading. Because of infrared divergences, it is necessary to retain the quark mass until the last steps of the calculation and then extract the leading chiral behaviour. Using plane-wave methods with $m_u = m_d = m$ we find

$$2i\frac{32\pi\alpha m_q^2}{D^2 q^2}\langle\alpha G^2\rangle\left[m^2(8-4D)K_1 - 2DK_2 + (D^2-4D+8)K_3\right] \ , \tag{57}$$

[7] Ref. [14] only provides the final result for the scalar case; Eq. (48) presents the results in a form similar to the pseudoscalar results contained in [14].

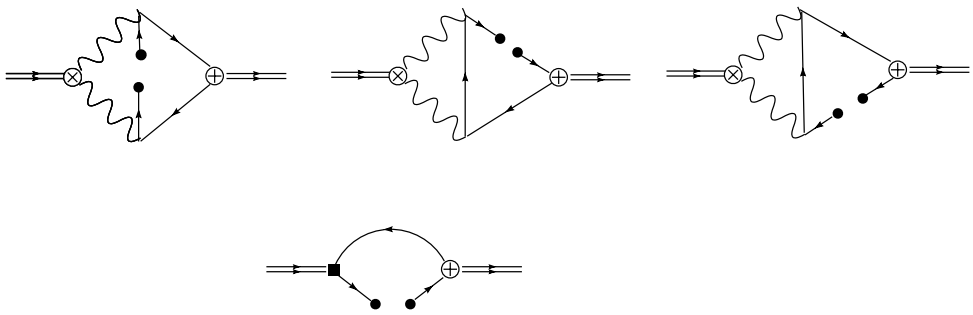

Figure 2: Leading order quark condensate diagrams for the non-diagonal correlation function. The solid circles on the quark lines denote insertion of plane-wave states or coordinate space vacuum expectation values for evaluation of the operator-product expansion coefficients. All other notations are identical to Fig. 1.

where

$$K_1 = \int \frac{d^D k}{(2\pi)^D} \frac{1}{(k^2-m^2)^2\,[(q-k)^2-m^2]} = \frac{i}{16\pi^2}\frac{1}{q^2\sqrt{1-4m^2/q^2}} \log\left[\frac{\sqrt{1-4m^2/q^2}+1}{\sqrt{1-4m^2/q^2}-1}\right] , \tag{58}$$

$$K_2 = \int \frac{d^D k}{(2\pi)^D} \frac{1}{(k^2-m^2)^2} = \frac{i}{16\pi^2}\left(\frac{m^2}{4\pi\nu^2}\right)^{\epsilon} \frac{\Gamma(2+\epsilon)\Gamma(-\epsilon)}{\Gamma(2+\epsilon)} , \tag{59}$$

$$\begin{aligned} K_3 &= \int \frac{d^D k}{(2\pi)^D} \frac{1}{(k^2-m^2)\,[(q-k)^2-m^2]} \\ &= \frac{i}{16\pi^2}\left(-\frac{1}{\epsilon} - \gamma - \log\left(\frac{m^2}{4\pi\nu^2}\right) + 2 - \sqrt{1-4m^2/q^2}\log\left[\frac{\sqrt{1-4m^2/q^2}+1}{\sqrt{1-4m^2/q^2}-1}\right]\right) . \end{aligned} \tag{60}$$

The divergences in K_3 and K_2 cancel, leaving a finite result as required given the m^2/q^2 pre-factor. The logarithmic correction from K_1 is seen to be subleading compared with the logarithmic correction from K_3. Thus the leading-chiral gluon condensate contribution to the non-diagonal correlator is

$$\frac{2\alpha m_q^2}{\pi Q^2}\langle \alpha G^2\rangle \left[3 - \log\left(\frac{Q^2}{m_q^2}\right)\right] . \tag{61}$$

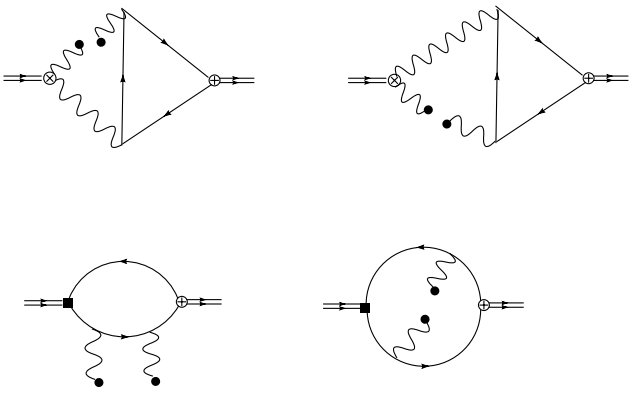

Figure 3: Leading order gluon condensate diagrams for the non-diagonal correlation function. The solid circles on the gluon lines denote insertion of plane-wave states for evaluation of the operator-product expansion coefficients. All other notations are identical to Fig. 1.

An additional subtlety must be addressed before we can accept (61) as definitive. It is known that the naively-calculated $\langle \alpha G^2\rangle$ results may differ from the actual $\langle \alpha G^2\rangle$ contributions when the quark mass is retained to obtain subleading mass corrections in the gluon condensate contributions [33]. The resolution of this problem is related to operator mixing; the coefficient of the operator G^2 receives a correction of

$$\frac{\alpha}{12m} C_{QQ} , \tag{62}$$

where C_{QQ} is the coefficient of the quark condensate $\langle\bar{q}q\rangle$ [33]. In our case, $C_{QQ} \sim m\alpha^2$ which provides a $\sim \alpha^3$ correction to the coefficient of G^2, representing a subleading correction compared with (61). Hence we conclude that no further calculation is needed to obtain the leading gluon condensate corrections.

Finally, the result of our calculation for the single instanton [24] contributions to the non-diagonal correlator in the dilute instanton liquid model [19] are:

$$\Pi_{gq}^{inst}\left(Q^2\right) = -8\sqrt{3n_c}m_q\alpha\rho Q^2\sqrt{\rho^2Q^2}K_1\left(\sqrt{\rho^2Q^2}\right)K_2\left(\sqrt{\rho^2Q^2}\right) \ , \tag{63}$$

where K_n is a modified Bessel function in the conventions of [27].

Combining Eqs. (55), (56), (61), and (63) we have the leading-order chiral and α contributions to the non-diagonal correlation function of gluonic and (non-strange) $I = 0$ quark currents:

$$\begin{aligned}\Pi_{gq}\left(Q^2\right) =& m_q^2Q^2\left[A_0L + A_1L^2\right] + m_q\langle\bar{q}q\rangle C_0\log\left(\frac{Q^2}{\nu^2}\right) + m_q^2\langle\alpha G^2\rangle\frac{1}{Q^2}\left[B_0 + B_1\log\left(\frac{Q^2}{m_q^2}\right)\right] \\ &- 8\sqrt{3n_c}m_q\alpha\rho Q^2\sqrt{\rho^2Q^2}K_1\left(\sqrt{\rho^2Q^2}\right)K_2\left(\sqrt{\rho^2Q^2}\right)\end{aligned} \tag{64}$$

$$C_0 = -8\pi\left(\frac{\alpha}{\pi}\right)^2 \ , \tag{65}$$

$$B_0 = 6\frac{\alpha}{\pi} \ , \ B_1 = -2\frac{\alpha}{\pi} \ , \tag{66}$$

along with A_0, A_1 given in (55). From the correlation function, the $k = 0$ GSR can be calculated as outlined in Section 2:

$$\begin{aligned}G_0^{(gq)}\left(\hat{s},\tau,s_0\right) =& \frac{m_q^2}{\sqrt{4\pi\tau}}\int_0^{s_0}dt\,\exp\left[-\frac{\left(t-\hat{s}\right)^2}{4\tau}\right]t\left(A_0 + 2A_1\log\left[\frac{t}{4\pi\sqrt{\tau}}\right]\right) \\ &- C_0m_q\langle\bar{q}q\rangle\frac{1}{\sqrt{4\pi\tau}}\int_0^{s_0}dt\,\exp\left[-\frac{\left(t-\hat{s}\right)^2}{4\tau}\right] + B_0m_q^2\langle\alpha G^2\rangle\frac{1}{\sqrt{4\pi\tau}}\exp\left(-\frac{\hat{s}^2}{4\tau}\right) \\ &+ B_1m_q^2\langle\alpha G^2\rangle\frac{1}{\sqrt{4\pi\tau}}\lim_{\eta\to 0}\left\{\int_\eta^{s_0}dt\,\frac{1}{t}\exp\left[-\frac{\left(t-\hat{s}\right)^2}{4\tau}\right] + \log\left(\frac{\eta}{m_q^2}\right)\exp\left(-\frac{\hat{s}^2}{4\tau}\right)\right\} \\ &+ 2\sqrt{3n_c}\pi m_q\alpha\rho^2\frac{1}{\sqrt{4\pi\tau}}\int_0^{s_0}dt\,\exp\left[-\frac{\left(t-\hat{s}\right)^2}{4\tau}\right]t\sqrt{t}\left[J_1\left(\rho\sqrt{t}\right)Y_2\left(\rho\sqrt{t}\right) + J_2\left(\rho\sqrt{t}\right)Y_1\left(\rho\sqrt{t}\right)\right]\end{aligned} \tag{67}$$

where in practice, the limit $\eta \to 0$ is implemented numerically with values of $\eta < 10^{-4}$ in GeV units. The normalized GSR is defined by

$$N_0^{(gq)}\left(\hat{s},\tau,s_0\right) = \frac{G_0^{(gq)}\left(\hat{s},\tau,s_0\right)}{M_0^{(gq)}\left(\tau,s_0\right)} \ , \ M_0^{(gq)}(\tau,s_0) = \int_{-\infty}^{\infty}G_0^{(gq)}(\hat{s},\tau,s_0)\,\mathrm{d}\,\hat{s} \ . \tag{68}$$

In Eqs. (67) m_q and α are implicitly the leading-order versions of the running quantities (36) and (38) evaluated at the scale $\nu^2 = \sqrt{\tau}$.

Since a low-energy theorem exists for the non-diagonal correlator [13]

$$\Pi_{gq}(0) = \frac{48\pi}{9}m_q\langle\bar{q}q\rangle \ , \tag{69}$$

the LET-sensitive $k = -1$ GSR is also relevant. Again using the methods outlined in Section 2 the corresponding

results for the $k=-1$ GSR are

$$\begin{aligned}
G_{-1}^{(gq)}\left(\hat{s},\tau,s_0\right) =& \frac{m_q^2}{\sqrt{4\pi\tau}}\int_0^{s_0} dt\, \exp\left[-\frac{\left(t-\hat{s}\right)^2}{4\tau}\right]\left(A_0+2A_1\log\left[\frac{t}{4\pi\sqrt{\tau}}\right]\right) \\
&- C_0 m_q\langle\bar{q}q\rangle \lim_{\eta\to 0}\left\{\int_\eta^{s_0} dt\,\frac{1}{t}\exp\left[-\frac{\left(t-\hat{s}\right)^2}{4\tau}\right]+\log\left(\frac{\eta}{\sqrt{\tau}}\right)\exp\left(-\frac{\hat{s}^2}{4\tau}\right)\right\} \\
&+ B_1 m_q^2\langle\alpha G^2\rangle\frac{1}{\sqrt{4\pi\tau}}\lim_{\eta\to 0}\left\{\int_\eta^{s_0} dt\,\frac{1}{t^2}\exp\left[-\frac{\left(t-\hat{s}\right)^2}{4\tau}\right]-\frac{1}{\eta}\exp\left(-\frac{\hat{s}^2}{4\tau}\right)\right\} \\
&+ 2\sqrt{3n_c}\pi m_q\alpha\rho^2\frac{1}{\sqrt{4\pi\tau}}\int_0^{s_0} dt\,\exp\left[-\frac{\left(t-\hat{s}\right)^2}{4\tau}\right]\sqrt{t}\left[J_1\left(\rho\sqrt{t}\right)Y_2\left(\rho\sqrt{t}\right)+J_2\left(\rho\sqrt{t}\right)Y_1\left(\rho\sqrt{t}\right)\right] \\
&- \frac{1}{\sqrt{4\pi\tau}}\exp\left(-\frac{\hat{s}^2}{4\tau}\right)\frac{16\sqrt{3n_c}m_q\alpha}{\rho}\ .
\end{aligned} \tag{70}$$

Note that the last term in (70) has a functional dependence identical to the LET term in (19), and hence there is an LET-like instanton contribution for the non-diagonal GSR similar to the diagonal gluonic case [7]. The $k=-1$ NGSR is defined by

$$N_{-1}^{(gq)}\left(\hat{s},\tau,s_0\right)=\frac{G_{-1}^{(gq)}\left(\hat{s},\tau,s_0\right)+\frac{1}{\sqrt{4\pi\tau}}\exp\left(\frac{-\hat{s}^2}{4\tau}\right)\Pi_{gq}(0)}{M_{-1}^{(gq)}\left(\tau,s_0\right)+\Pi_{gq}(0)}\ ,\ M_{-1}^{(gq)}(\tau,s_0)=\int_{-\infty}^{\infty}G_{-1}^{(gq)}(\hat{s},\tau,s_0)\,\mathrm{d}\,\hat{s}\ . \tag{71}$$

The non-diagonal correlator and its associated GSR have quite distinct chiral behaviour compared with the diagonal correlators. In the diagonal case, the perturbative, condensate, and instanton corrections all appear with identical powers of the quark mass. However, in the off-diagonal case the perturbative and gluon condensate corrections are chirally-suppressed compared with the quark condensate and instanton terms. The physical implications of this result will be discussed below.

4 Analysis of Gaussian Sum-Rules for $q\bar{q}$ and Gluonic Currents

The general strategy for analysis of NGSRs is fitting the QCD prediction with a parameterized model for $\rho^{\mathrm{had}}(t)$ in (21). Correlation functions of vector and axial-vector $q\bar{q}$ currents can be directly related to experimental data (*e.g.,* $R(s)$), but in the case of gluonium there is no direct connection with experimental observables. The narrow resonance approximation is the most common choice made for Laplace sum-rule analyses of gluonium, with either a single (narrow) resonance [6, 23, 34, 35] to examine the dominant gluonic state or two (narrow) resonances [4, 5, 36] to explore the possibility of $q\bar{q}$-gluonium mixtures. Laplace sum-rule gluonium analyses which go beyond the narrow width approximation include a single Breit-Wigner resonance skewed by kinematic factors [37], and an interpolation between the LET and continuum behaviour [16]. Finite-energy sum-rule analyses of scalar gluonium that incorporate resonance widths include step functions [38] and Breit-Wigner resonances [39] with kinematic skewing.[8]

GSR analyses of gluonium have employed single and double narrow resonance models in addition to a variety of models that incorporate resonance widths [7, 9]. However, since the gaussian kernel in (1) has a QCD-limited width of $2\sqrt{\tau}\geq 2\,\mathrm{GeV}^2$, one would expect that there is insufficient resolution to observe resonance width effects and hence the narrow resonance may be an appropriate approximation. Such an approximation is clearly desirable for fitting the QCD prediction to the resonance model in (21) for multiple resonances.

To explore the effect of the narrow width approximation, we consider the following models for a resonance of mass m: a narrow resonance

$$\frac{1}{\pi}\rho^{\mathrm{nr}}=f^2\delta\left(t-m^2\right)\ , \tag{72}$$

a structureless square pulse of width $2m\Gamma$

$$\frac{1}{\pi}\rho^{\mathrm{sp}}(t)\equiv\frac{f_{\mathrm{sp}}^2}{2m\Gamma}\left[\theta\left(t-m^2+m\Gamma\right)-\theta\left(t-m^2-m\Gamma\right)\right]\ , \tag{73}$$

[8] Ref. [39] also uses the Gaussian sum-rule diffusion equation (16) analysis to constrain the QCD continuum. As discussed in Section 2, our approach based on NGSRs provides information that is *independent* of this duality constraint.

and a gaussian shape

$$\rho^{\rm gr}(t) \equiv f_g^2 \exp\left[-\frac{\left(t-m^2\right)^2}{2\gamma^2}\right] . \tag{74}$$

For the square pulse the quantity Γ has a direct analogy with the Breit-Wigner width $\Gamma = \Gamma_{BW}$; for the gaussian shape the relation is $\Gamma_{BW} = \sqrt{2\log(2)}\gamma/m$. The contribution of these models to the quantity appearing on the right-hand side of (21)

$$N_0{}^{\rm had}(\hat{s},\tau) = \frac{\frac{1}{\sqrt{4\pi\tau}}\int_{t_0}^{\infty} t^k \exp\left[\frac{-(\hat{s}-t)^2}{4\tau}\right]\rho^{\rm had}(t)\,{\rm d}\,t}{\int_{t_0}^{\infty} t^k \rho^{\rm had}(t)\,{\rm d}\,t} \tag{75}$$

can be calculated in closed form [7]:

$$N_0^{\rm nr}(\hat{s},\tau) = \frac{1}{\sqrt{4\pi\tau}} \exp\left[-\frac{\left(\hat{s}-m^2\right)^2}{4\tau}\right] , \tag{76}$$

$$N_0^{\rm sp}(\hat{s},\tau) = \frac{1}{4m\Gamma}\left[{\rm erf}\left(\frac{\hat{s}-m^2+m\Gamma}{2\sqrt{\tau}}\right) - {\rm erf}\left(\frac{\hat{s}-m^2-m\Gamma}{2\sqrt{\tau}}\right)\right] , \tag{77}$$

$$N_0^{\rm gr}(\hat{s},\tau) = \frac{1+{\rm erf}\left(\frac{\hat{s}\gamma^2+2m^2\tau}{2\gamma\sqrt{\tau}\sqrt{\gamma^2+2\tau}}\right)}{\sqrt{2\pi}\sqrt{\gamma^2+2\tau}\left[1+{\rm erf}\left(\frac{m^2}{\sqrt{2}\gamma}\right)\right]} \exp\left[-\frac{\left(\hat{s}-m^2\right)^2}{2\left(\gamma^2+2\tau\right)}\right] \quad . \tag{78}$$

As argued above, we see that in the limits $2\sqrt{\tau} \gg m\Gamma$ and $2\sqrt{\tau} \gg \gamma$ the models (77) and (78) incorporating a resonance width will be indistinguishable from the narrow-resonance case. Fig. 4 compares (76)–(78) along with a numerical approximation for a Breit-Wigner shape when $m = 1\,{\rm GeV}$ and $\Gamma_{BW} = 300\,{\rm MeV}$. The Figure illustrates that the resolution of the gaussian kernel is the dominant effect; resonance width effects correspond to a slight broadening compared to the narrow resonance case. Furthermore, resonance width effects would not alter the fitted value of the resonance mass. This has been explored by finding the mass M in the various models with $\Gamma_{BW} = 300\,{\rm MeV}$ that provides the least-squares fit to a $m = 1\,{\rm GeV}$ narrow resonance. In all cases (square pulse, gaussian shape, Breit-Wigner) the fitted mass M coincides with $1\,{\rm GeV}$.

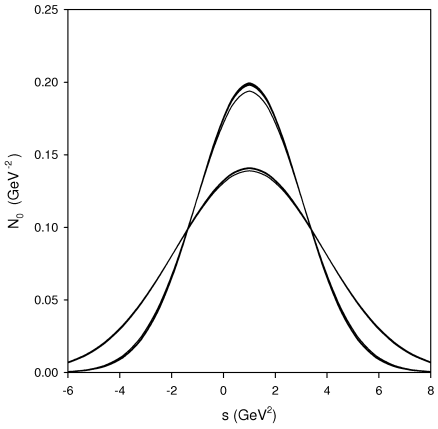

Figure 4: Comparison between $N_0\,(\hat{s},\tau)$ for $m = 1\,{\rm GeV}$ in the narrow resonance model and the square pulse, gaussian, and Breit-Wigner models with $\Gamma_{BW} = 300\,{\rm MeV}$. The upper set of curves are for $\tau = 2\,{\rm GeV}^4$ and the bottom set of curves is for $\tau = 4\,{\rm GeV}^4$.

Our observation that the mass would be unaltered when fitting the various models to a QCD prediction can be understood by noting that the peaks are aligned in Fig. 4. However, if one introduces a kinematic distortion of t^2 into Eqs. (73)–(74) as in Refs. [13, 37, 38, 39] then the peak position will be shifted above $t = m^2$. For example, the

kinematically-skewed generalizations of Eqs. (73)–(74) are

$$\frac{1}{\pi}\rho^{\rm ssp}(t) \equiv f_{\rm ssp}^2 \frac{t^2}{2m^3\Gamma\left(m^2+\frac{\Gamma^2}{3}\right)}\left[\theta\left(t-m^2+m\Gamma\right)-\theta\left(t-m^2-m\Gamma\right)\right] \ , \tag{79}$$

$$\frac{1}{\pi}\rho^{\rm sg}(t) = f_{\rm sg}^2 t^2 \exp\left[-\frac{(t-m^2)^2}{2\gamma^2}\right] \ , \tag{80}$$

which lead to

$$\begin{aligned} N_0^{\rm ssp}(\hat{s},\tau) =& 2\tau\left(\hat{s}+m^2-m\Gamma\right)\exp\left[-\frac{\left(\hat{s}-m^2+m\Gamma\right)^2}{4\tau}\right] - 2\tau\left(\hat{s}+m^2+m\Gamma\right)\exp\left[-\frac{\left(\hat{s}-m^2-m\Gamma\right)^2}{4\tau}\right] \\ &+\sqrt{\pi\tau}\left[\hat{s}^2+2\tau\right]\left(\mathrm{erf}\left[\frac{\hat{s}-m^2+m\Gamma}{2\sqrt{\tau}}\right]-\mathrm{erf}\left[\frac{\hat{s}-m^2-m\Gamma}{2\sqrt{\tau}}\right]\right) \end{aligned} \tag{81}$$

$$\begin{aligned} E\,N_0^{\rm sg}(\hat{s},\tau) =& \,4\exp\left[-\frac{\hat{s}^2\gamma^2+2\tau m^4}{4\tau\gamma^2}\right]\gamma\sqrt{\tau}\sqrt{\gamma^2+2\tau}(\hat{s}\gamma^2+2\tau m^2) \\ &+2\sqrt{\pi}\exp\left[-\frac{(\hat{s}-m^2)^2}{2(\gamma^2+2\tau)}\right](\hat{s}^2\gamma^4+4\hat{s}\gamma^2m^2\tau+4m^4\tau^2+2\tau\gamma^4+4\tau^2\gamma^2) \\ &\times\left[1+\mathrm{erf}\left(\frac{\hat{s}\gamma^2+2\tau m^2}{2\gamma\sqrt{\tau}\sqrt{\gamma^2+2\tau}}\right)\right] \ , \end{aligned} \tag{82}$$

where

$$E = \sqrt{2\pi}(m^4+\gamma^2)\left[1+\mathrm{erf}\left(\frac{m^2}{\sqrt{2}\gamma}\right)\right]+2m^2\gamma\exp\left(-\frac{m^4}{2\gamma^2}\right)\sqrt{\pi}(\gamma^2+2\tau)^{5/2} \ . \tag{83}$$

In fact, the skewed square pulse is the model used in Ref. [38] for a finite-energy sum-rule analysis. If we now fit Eqs. (81) and (82) with $\Gamma_{BW} = 300\,\mathrm{MeV}$ to find the mass M that provides the least-squares fit to a 1 GeV narrow resonance, M is found to be slightly less than 1 GeV (0.93, GeV and 0.98 GeV respectively). Fig. 5 shows the best fits; the narrow resonance still provides an excellent approximation in the presence of a kinematic skewing factor once the mass shift is taken into account.

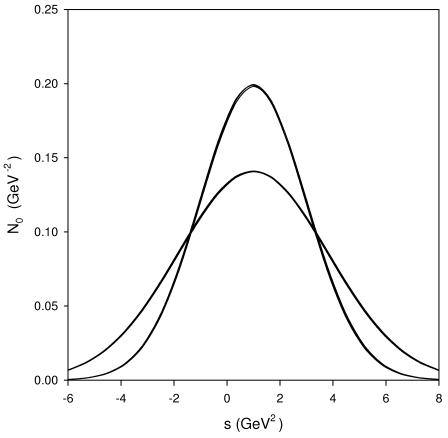

Figure 5: Comparison between $N_0(\hat{s},\tau)$ for $m = 1\,\mathrm{GeV}$ in the skewed square pulse and gaussian models with $\Gamma_{BW} = 300\,\mathrm{MeV}$ along with the best fit of a single narrow resonance to each model. The upper set of curves are for $\tau = 2\,\mathrm{GeV}^4$ and the bottom set of curves is for $\tau = 4\,\mathrm{GeV}^4$.

Thus we conclude that for purposes of a least-squares fitting methodology, the narrow-width model provides a good approximation to a variety of resonance models that incorporate resonance widths. However, there exists the possibility that the fitted mass resulting from fitting the narrow-width model may over-estimate the actual resonance mass by no more than 10%, *i.e.*, the narrow-width approximation provides an *upper bound* on the resonance mass in more complicated models [40].

In summary, the methodology we will employ to study $q\bar{q}$-gluonium states including the possibility of mixing, is to fit the QCD prediction to the double narrow resonance model for the NGSRs in the two diagonal (qq, gg) cases and the non-diagonal case. In general, this methodology will take the form

$$\frac{1}{\pi}\rho^{\rm had}(t) = f_1^2\delta(t-m_1^2) + f_2^2\delta(t-m_2^2) \ , \tag{84}$$

$$N_0^{\rm QCD}(\hat{s},\tau,s_0) = \frac{1}{\sqrt{4\pi\tau}}\left\{ r_1 \exp\left[-\frac{(\hat{s}-m_1^2)^2}{4\tau}\right] + r_2 \exp\left[-\frac{(\hat{s}-m_2^2)^2}{4\tau}\right]\right\} \ , \tag{85}$$

$$r_1 = \frac{f_1^2}{f_1^2+f_2^2} \ , \ r_2 = \frac{f_2^2}{f_1^2+f_2^2} \ , \ r_1+r_2 = 1 \ . \tag{86}$$

where f_1, f_2 denote the couplings of the resonances to the currents under consideration. A least squares fit of the $\hat{s}$, τ dependence on the two sides of (85) therefore involves minimization with respect to four parameters: the QCD continuum s_0, the two resonance masses (m_1, m_2), and either r_1 or r_2 because of the $r_1+r_2=1$ normalization constraint. The three NGSRs [see Eqs. (31), (37), (67)] involving all possible combinations of the $q\bar{q}$ and gluonic currents will be analyzed separately. This independent analysis of each channel is essential because a signal of states that are $q\bar{q}$-gluonic mixtures would be the self-consistent appearance of states of the same mass in *all three* cases since such mixtures would necessarily couple to both the gluonic and $q\bar{q}$ currents.

The QCD input parameters appearing within the NGSRs will now be specified. For the gluon condensate we employ the (central) value from [41]

$$\langle \alpha G^a_{\ \mu\nu} G^{a\mu\nu}\rangle = \langle \alpha G^2\rangle = (0.07 \pm 0.01)\,{\rm GeV}^4 \quad , \tag{87}$$

and the quark condensate is determined by the PCAC relation

$$m_q\langle\bar{q}q\rangle = -\frac{1}{2}f_\pi^2 m_\pi^2 \ , \ f_\pi = 93\,{\rm MeV}\,. \tag{88}$$

The dimension six gluon condensate (33) can be related to the value of $\langle\alpha G^2\rangle$ using instanton techniques (see [23, 29])

$$\langle\mathcal{O}_6\rangle = (0.27\,{\rm GeV}^2)\langle\alpha G^2\rangle \quad . \tag{89}$$

Further, by invoking vacuum saturation in conjunction with the heavy quark expansion, Ref. [42] has also related the dimension eight gluon condensate (34) to $\langle\alpha G^2\rangle$ through

$$\langle\mathcal{O}_8\rangle = \frac{9}{16}\left(\langle\alpha G^2\rangle\right)^2 \quad . \tag{90}$$

We use $f_{vs}=1.5$ as a central value to accommodate the observed deviations from vacuum saturation in the dimension six quark condensates (41) [43]. In addition, the dilute instanton liquid (DIL) model [19] parameters (which have an estimated uncertainty of about 15%)

$$n_c = 8.0\times 10^{-4}\ {\rm GeV}^4 \quad , \quad \rho = \frac{1}{0.6}\ {\rm GeV}^{-1} \tag{91}$$

will be employed. The NGSRs for the diagonal correlators do not require knowledge of the quark masses; in the diagonal gluonic case this occurs because the leading chiral behaviour is independent of the quark masses, while the diagonal $q\bar{q}$ case is proportional to m_q^2 and hence the quark mass dependence cancels when forming the NGSR. However, the non-diagonal case has terms of differing chiral order and therefore requires input of the quark mass. Unfortunately, m_q is not known very accurately; we will use the Particle Data Group range for the 2 GeV $\overline{\rm MS}$ mass [1]:

$$2.5\,{\rm MeV} < m_q(2\,{\rm GeV}) < 5.5\,{\rm MeV}\ . \tag{92}$$

The implications of the large uncertainty in m_q within our analysis will be discussed in more detail below.

We begin with the diagonal gluonic-gluonic case. As argued in Ref. [7] the LET-sensitive $k=-1$ GSR shows a strong dependence of the QCD input parameters (particularly the instanton parameters and gluon condensate) compared to the $k=0$ GSR. Our current analysis will therefore focus on the $k=0$ case.[9] In Ref. [7] numerically-efficient techniques involving the τ dependence of the $\hat{s}$ peak position were developed to extract the resonance

[9] The qualitative consistency between the $k=0$ and $k=-1$ cases has been demonstrated for Laplace sum-rules [19, 20]; instanton effects are an essential feature of these works.

and QCD continuum parameters. The numerical efficiency gained from these techniques allowed exploration of a variety of resonance models, including the double narrow resonance model which resulted in the central values $s_0 = 2.3\,\mathrm{GeV}^2$, $m_1 = 0.98\,\mathrm{GeV}$, $m_2 = 1.4\,\mathrm{GeV}$, $r_1^{(gg)} = 0.28$, and $r_2^{(gg)} = 0.72$ [7, 9]. As an independent check of these diagonal gluonic results for this paper, we have performed a least-squares fit between the two sides of (85) in the range $-4\,\mathrm{GeV}^2 < \hat{s} < 8\,\mathrm{GeV}^2$ and $2\,\mathrm{GeV}^4 < \tau < 4\,\mathrm{GeV}^4$ resulting in $s_0 = 2.30\,\mathrm{GeV}^2$, $m_1 = 0.951\,\mathrm{GeV}$, $m_2 = 1.41\,\mathrm{GeV}$, $r_1^{(gg)} = 0.303$, and $r_2^{(gg)} = 0.697$. The close agreement between the predicted resonance parameters and QCD continuum in these two different approaches validates the methodologies. As illustrated in Fig. 6, the resulting fit between the QCD prediction and double narrow-resonance model is excellent; there is no suggestion of resonance-width effects that would lead to differences between the QCD prediction and the phenomenological model on a scale similar to that of Fig. 4. The uncertainties associated with the QCD input parameters have been found to be 10% for $r_2^{(gg)}$ and 0.2 GeV for the masses, with a correlated effect in the masses that lead to a relatively stable mass splitting $m_1 - m_2 \approx 0.5\,\mathrm{GeV}$ with an uncertainty of 0.03 GeV [7].

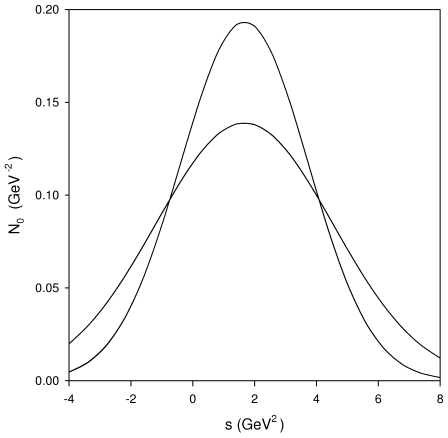

Figure 6: Comparison of the theoretical prediction for the normalized GSR $N_0^{(gg)}(\hat{s}, \tau, s_0)$ with the double narrow resonance phenomenological model for the optimized value of the continuum s_0 and resonance parameters (m_1, m_2, r_1). The upper set of curves are for $\tau = 2\,\mathrm{GeV}^4$ and the bottom set of curves is for $\tau = 4\,\mathrm{GeV}^4$. The phenomenological and QCD predictions cannot be distinguished in the plots because they overlap almost completely.

The diagonal $q\bar{q}$-$q\bar{q}$ ($I = 0$) case does not have the complexity of a LET-sensitive sum-rule, so $k = 0$ is the lowest-weighted GSR that can be analyzed. The central values obtained from the $\hat{s}$ peak-position analysis are $s_0 = 2.6\,\mathrm{GeV}^2$, $m_1 = 0.97\,\mathrm{GeV}$, $m_2 = 1.4\,\mathrm{GeV}$, $r_1^{(qq)} = 0.63$, and $r_2^{(qq)} = 0.37$ [8, 9]. As in the diagonal gluonic case, we have performed a least-squares fit between the two sides of (85) in the range $-4\,\mathrm{GeV}^2 < \hat{s} < 8\,\mathrm{GeV}^2$ and $2\,\mathrm{GeV}^4 < \tau < 4\,\mathrm{GeV}^4$ resulting in $s_0 = 2.348\,\mathrm{GeV}^2$, $m_1 = 0.943\,\mathrm{GeV}$, $m_2 = 1.41\,\mathrm{GeV}$, $r_1^{(qq)} = 0.593$, and $r_2^{(qq)} = 0.407$. Fig. 7 again shows excellent agreement of the resulting fit between the QCD prediction and double narrow-resonance model. Once again, there is no suggestion of anomalous differences between the QCD prediction and the phenomenological model indicative of substantial resonance-width effects. The uncertainty associated with $r_1^{(qq)}$ is 10%, comparable to the diagonal gluonic case, but the masses show less dependence on the QCD input parameters than the diagonal gluonic case with uncertainties of 0.05 GeV. The uncertainty in the masses is correlated as in the gluonic case; the mass difference of approximately 0.5 GeV between the two states is relatively stable.

The remarkable agreement between the resonance masses resulting from the diagonal gluonic and diagonal $q\bar{q}$ NGSRs suggests the existence of states with masses of $\approx 1.0\,\mathrm{GeV}$ and $\approx 1.4\,\mathrm{GeV}$ which are gluonium-$q\bar{q}$ mixtures, with the heavier state being slightly more gluonic because of its stronger coupling in the gluonic channel and a weaker coupling in the $q\bar{q}$ channel. The results also indicate that the mixing is rather strong because r_1 and r_2 are not appreciably different, and hence the non-diagonal correlator must also contain clear signals of this strong mixing to validate this scenario.

Before proceeding with a detailed analysis of the non-diagonal correlator, we consider the approximate scales associated with the couplings of the resonances to the gluonic and scalar currents. The perturbative corrections in the diagonal correlators (31) and (37) imply that

$$f_g^2 \sim \left(\frac{\alpha}{\pi}\right)^2 M^4 \ , \ f_q^2 \sim m_q^2 M^2 \ , \tag{93}$$

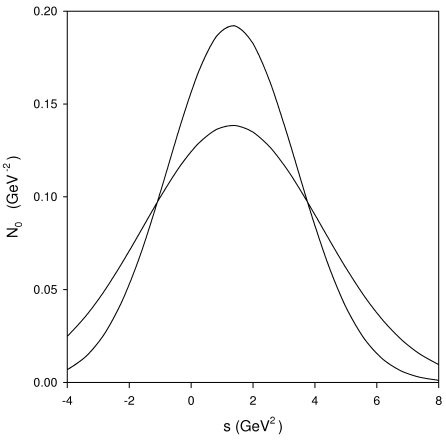

Figure 7: Comparison of the theoretical prediction for the normalized GSR $N_0^{(qq)}(\hat{s},\tau,s_0)$ with the double narrow resonance phenomenological model for the optimized value of the continuum s_0 and resonance parameters (m_1, m_2, r_1). The upper set of curves are for $\tau = 2\,\mathrm{GeV}^4$ and the bottom set of curves is for $\tau = 4\,\mathrm{GeV}^4$. The phenomenological and QCD predictions cannot be distinguished in the plots because they overlap almost completely.

where f_g and f_q respectively denote the resonance couplings to the gluonic and $q\bar{q}$ currents and M is a characteristic sum-rule scale of order $M \sim 1\,\mathrm{GeV}$. In the simplest single-angle mixing scenario, the non-diagonal correlator will be proportional to $f_g f_q \sin 2\theta$ where θ is the mixing angle. The perturbative corrections to the non-diagonal correlator (67) then imply

$$f_g f_q \sin 2\theta \sim m_q^2 \left(\frac{\alpha}{\pi}\right)^2 M^2 \ . \tag{94}$$

Combining (93) and (94) then leads to a chirally-suppressed mixing angle

$$\sin 2\theta \sim \frac{\alpha}{\pi}\frac{m_q}{M} \ll 1 \ . \tag{95}$$

The apparent contradiction between the strong mixing found in the GSRs for the diagonal correlators and the basic perturbative scales in the non-diagonal GSR is resolved by a detailed analysis of the non-diagonal case. We first define the leading $\mathcal{O}(m_q)$ chiral terms in (67) as

$$\begin{aligned}\chi_0^{(gq)}(\hat{s},\tau,s_0) = &-C_0 m_q \langle\bar{q}q\rangle \frac{1}{\sqrt{4\pi\tau}} \int_0^{s_0} dt\, \exp\left[-\frac{(t-\hat{s})^2}{4\tau}\right] \\ &+ 2\sqrt{3n_c}\pi m_q \alpha\rho^2 \frac{1}{\sqrt{4\pi\tau}} \int_0^{s_0} dt\, \exp\left[-\frac{(t-\hat{s})^2}{4\tau}\right] t\sqrt{t}\left[J_1\left(\rho\sqrt{t}\right)Y_2\left(\rho\sqrt{t}\right) + J_2\left(\rho\sqrt{t}\right)Y_1\left(\rho\sqrt{t}\right)\right] \ .\end{aligned} \tag{96}$$

Fig. 8 demonstrates that these leading chiral terms are actually the dominant contribution to the non-diagonal NGSR, avoiding the chiral suppression occurring in (95). We thus have the intriguing result that the underlying mixing mechanism is fundamentally non-perturbative, *i.e.,* perturbative analyses do not provide the essential phenomenological scales.

Because of the PCAC relation (88), the quark condensate term in (96) is independent of m_q, so in principle $N_0^{(gq)}$ could be strongly dependent on m_q. Fig. 9 shows that this is not the case; the chiral contributions to $N_0^{(gq)}$ are relatively insensitive to the range (92) for m_q. However, Fig. 10 shows that this is not the case for the LET-sensitive NGSR $N_{-1}^{(gq)}$ which exhibits strong dependence on m_q. Thus we focus our analysis on the $k = 0$ NGSR $N_0^{(gq)}$ as it is less affected by quark-mass uncertainties.

Our detailed analysis of the non-diagonal GSR begins with an exploration of its consistency with the results of

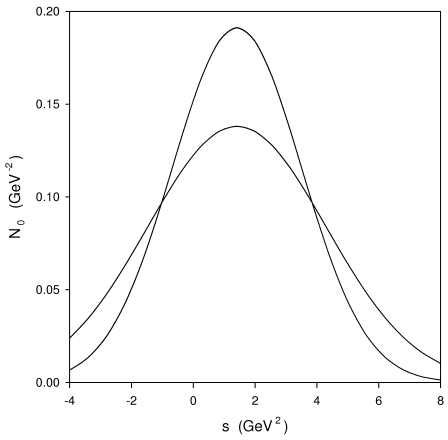

Figure 8: Comparison of the complete non-diagonal NGSR $N_0^{(gq)}(\hat{s},\tau,s_0)$ with that constructed using only the leading order chiral contributions (quark condensate and instanton terms) given in (96). Central values of the QCD input parameters have been employed along with $s_0 = 2.5\,\mathrm{GeV}^2$. The upper set of curves are for $\tau = 2\,\mathrm{GeV}^4$ and the bottom set of curves is for $\tau = 4\,\mathrm{GeV}^4$. The two curves overlap almost completely.

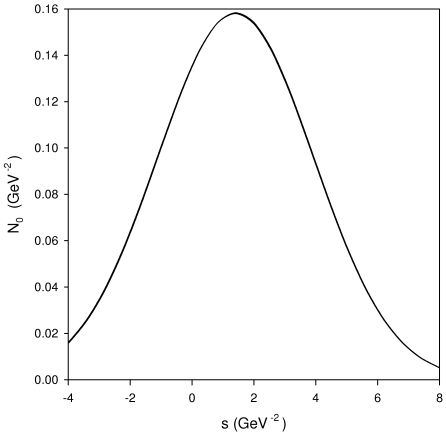

Figure 9: Comparison of the the NGSR $N_0^{(gq)}(\hat{s},\tau,s_0)$ for the upper and lower ranges of the quark mass specified in (92). Central values of the other QCD input parameters have been employed along with $\tau = 3\,\mathrm{GeV}^4$ and $s_0 = 2.5\,\mathrm{GeV}^2$. The two curves overlap almost completely.

the diagonal cases. In the double narrow resonance model, the non-diagonal NGSR has the form

$$N_0^{(gq)}(\hat{s},\tau,s_0) = \frac{1}{\sqrt{4\pi\tau}}\left\{r_1^{(gq)}\exp\left[-\frac{(\hat{s}-m_1^2)^2}{4\tau}\right] + r_2^{(gq)}\exp\left[-\frac{(\hat{s}-m_2^2)^2}{4\tau}\right]\right\}\ , \tag{97}$$

$$r_1^{(gq)} = \frac{f_{1g}f_{1q}}{f_{1g}f_{1q}+f_{2g}f_{2q}}\ ,\ r_2^{(gq)} = \frac{f_{2g}f_{2q}}{f_{1g}f_{1q}+f_{2g}f_{2q}}\ ,\ r_1^{(gq)}+r_2^{(gq)} = 1\ . \tag{98}$$

From the analysis of the diagonal cases, we have found $m_1 \approx 1\,\mathrm{GeV}$, $m_2 \approx 1.4\,\mathrm{GeV}$, and

$$r_1^{(gg)} = 0.303 = \frac{{f_{1g}}^2}{{f_{1g}}^2+{f_{2g}}^2}\ ,\ r_2^{(gg)} = 1-0.303 = \frac{{f_{2g}}^2}{{f_{1g}}^2+{f_{2g}}^2} \tag{99}$$

$$r_1^{(qq)} = 0.593 = \frac{{f_{1q}}^2}{{f_{1q}}^2+{f_{2q}}^2}\ ,\ r_2^{(qq)} = 1-0.593 = \frac{{f_{2q}}^2}{{f_{1q}}^2+{f_{2q}}^2}\ . \tag{100}$$

Thus the parameterization of the mixed gluonic-$\bar{q}q$ system has four couplings of the states to the various currents as in Ref. [5]. The four equations (99) and (100) representing the diagonal results determine the four couplings up to

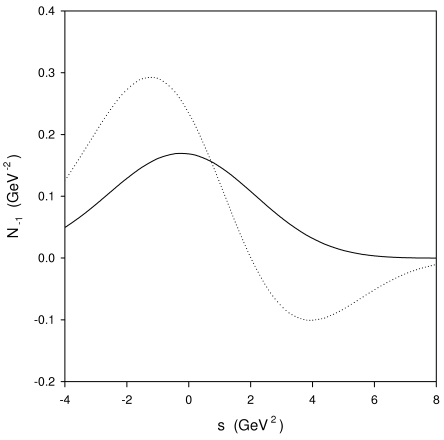

Figure 10: Comparison of the the NGSR $N_{-1}^{(gq)}(\hat{s},\tau,s_0)$ for the upper and lower ranges of the quark mass specified in (92). Central values of the other QCD input parameters have been employed along with $\tau = 3\,\mathrm{GeV}^4$ and $s_0 = 2.5\,\mathrm{GeV}^2$. The solid and dotted curves respectively correspond to the lower and upper bound on the quark mass.

an overall sign, leading to two possible solutions for the non-diagonal case

$$r_1^{(gq)} = \begin{cases} +0.443 \\ -3.899 \end{cases} . \tag{101}$$

Apart from the ambiguity arising from the sign of the couplings, all the phenomenological parameters in the non-diagonal NGSR (97) are determined except for the continuum s_0 which can be determined by performing a least-squares fit of the $\hat{s}$, τ dependence of (97) in the region range $-4\,\mathrm{GeV}^2 < \hat{s} < 8\,\mathrm{GeV}^2$ and $2\,\mathrm{GeV}^4 < \tau < 4\,\mathrm{GeV}^4$. The best fit for the two cases in (101) are shown in Figs. 11 and 12. From these Figures we see that the positive case in (101) is demonstrably most consistent with the QCD prediction.

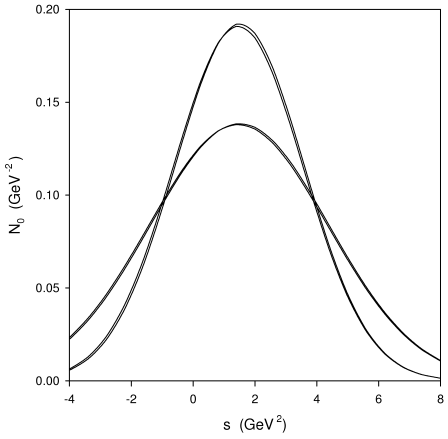

Figure 11: Comparison of the best fit of theoretical prediction for the normalized GSR $N_0^{(gq)}(\hat{s},\tau,s_0)$ to the double narrow resonance phenomenological model. Resonance parameters resulting from the analyses of the diagonal NGSRs have been employed (the solution $r_1 = 0.443$ from (101), along with $m_1 = 1\,\mathrm{GeV}$ and $m_2 = 1.4\,\mathrm{GeV}$). The optimized value of the continuum for these (inputted) resonance parameters is $s_0 = 2.8\,\mathrm{GeV}^2$. The upper set of curves are for $\tau = 2\,\mathrm{GeV}^4$ and the bottom set of curves is for $\tau = 4\,\mathrm{GeV}^4$. The phenomenological and QCD predictions overlap to a large extent.

At this point we can reach an important conclusion: the non-diagonal GSR is consistent with the results of the diagonal gluonic GSR analyses, providing strong evidence for a consistent scenario of mixed gluonic-$\bar{q}q$ states with

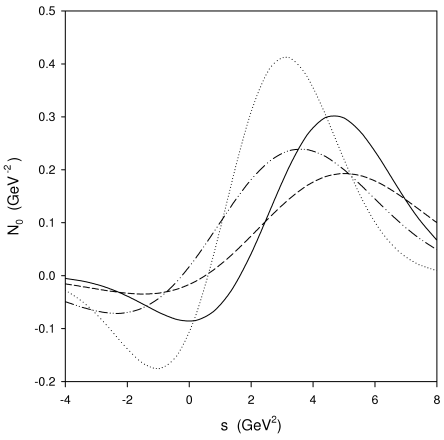

Figure 12: Comparison of the best fit of theoretical prediction for the normalized GSR $N_0^{(gq)}(\hat{s},\tau,s_0)$ to the double narrow resonance phenomenological model. Resonance parameters resulting from the analyses of the diagonal NGSRs have been employed (the solution $r_1 = -3.899$ from (101), along with $m_1 = 1\,\mathrm{GeV}$ and $m_2 = 1.4\,\mathrm{GeV}$). The optimized value of the continuum for these (inputted) resonance parameters is $s_0 = 5.2\,\mathrm{GeV}^2$. The solid and dashed curves represent $N_0^{(gq)}(\hat{s},\tau,s_0)$ and respectively correspond to $\tau = 2\,\mathrm{GeV}^4$ and $\tau = 4\,\mathrm{GeV}^4$. The dotted and dashed-dotted curves represent the double resonance model and respectively correspond to $\tau = 2\,\mathrm{GeV}^4$ and $\tau = 4\,\mathrm{GeV}^4$.

masses of $m_1 \approx 1\,\mathrm{GeV}$ and $m_2 \approx 1.4\,\mathrm{GeV}$ with the heavier state having a slightly larger gluonium content. A significant feature of our analysis is the nearly-identical masses that have resulted independently from the diagonal gluonic and diagonal $\bar{q}q$ cases. Although we have demonstrated that the non-diagonal case is consistent with these results, an independent analysis of the non-diagonal case would provide further confirmation of the gluonic-$\bar{q}q$ mixing scenario.

A least-squares fit of the $\hat{s}$, τ dependence of the non-diagonal NGSR (97) in the region range $-4\,\mathrm{GeV}^2 < \hat{s} < 8\,\mathrm{GeV}^2$ and $2\,\mathrm{GeV}^4 < \tau < 4\,\mathrm{GeV}^4$ results in $s_0 = 3.00\,\mathrm{GeV}^2$, $m_1 = 0.869\,\mathrm{GeV}$, $m_2 = 1.39\,\mathrm{GeV}$, $r_1^{(gq)} = 0.439$, $r_2^{(gq)} = 0.561$. Fig. 13 shows that the fit between the QCD prediction and phenomenological model is excellent, with no anomalous deviations indicative of effects from extremely wide resonances. The effect of varying the quark mass within the range (92) is minimal, so the dominant uncertainty in these predictions arise from the instanton parameters. One can estimate the effect of the instanton parameters by recognizing that the instanton contribution in (67) is proportional to

$$\int_0^{\rho^2 s_0} dw\, w\sqrt{w}\exp\Big[-\frac{\left(w-\rho^2\hat{s}\right)^2}{4\rho^4\tau}\Big]\left[J_1\left(w^2\right)Y_2\left(w^2\right)+J_2\left(w^2\right)Y_1\left(w^2\right)\right] = f\left(\rho^2\hat{s},\rho^4\tau,\rho^2 s_0\right)\ . \tag{102}$$

Thus if the instanton size is re-scaled by $\rho \to \rho/\xi$, its contribution to the NGSR is invariant under the scalings $s_0 \to \xi^2 s_0$, $\hat{s} \to \xi^2\hat{s}$, $\tau \to \xi^4\tau$. Now if these scaling laws are also applied to the double narrow resonance model on the right-hand side of (97), then it will also be invariant if the resonance parameters scale as $m_1 \to \xi^2 m_1$, $m_2 \to \xi^2 m_2$, $r_1^{(gq)} \to r_1^{(gq)}$, $r_2^{(gq)} \to r_2^{(gq)}$.[10] Thus the results of the best fit analysis will be approximately insensitive to changes in the instanton density n_c, the resonance strength will be relatively stable under variations in the instanton size, and the masses will scale proportionally with the instanton size. This implies that the 15% uncertainty in the instanton size will result in a systematic $\approx 15\%$ uncertainty (*i.e.,* each mass is shifted in the same direction, leading to the same 15% uncertainty in the mass splitting $m_1 - m_2$) in the mass predictions. It thus seems reasonable to conclude, taking other sources of theoretical uncertainty into account, that the pattern of uncertainty for the non-diagonal case is similar to that of the diagonal gluonic case; a $0.2\,\mathrm{GeV}$ correlated uncertainty in the mass predictions that leads to a relatively stable mass splitting that can deviate by 10% from the central value $m_1 - m_2 \approx 0.5\,\mathrm{GeV}$.

The results obtained from the diagonal and non-diagonal cases are summarized in Table 1. Taking into account the uncertainty in the fitted values of the resonance parameters for the diagonal and non-diagonal NGSRs, we see that the non-diagonal case leads to predictions that are consistent with those of the diagonal analyses, so that

[10]Note that overall factors, such as the normalization of the double resonance model and the instanton density, do not modify the NGSR and hence do not alter the scaling argument.

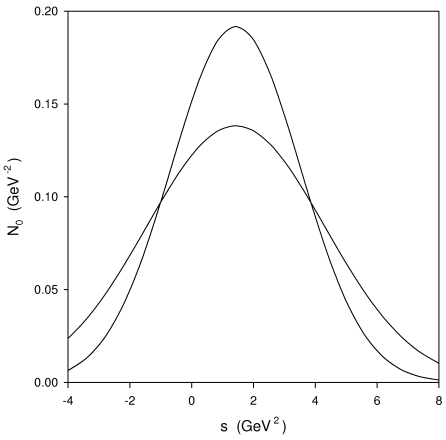

Figure 13: Comparison of the theoretical prediction for the non-diagonal NGSR $N_0^{(gq)}(\hat{s},\tau,s_0)$ with the double narrow resonance phenomenological model for the optimized value of the continuum s_0 and resonance parameters (m_1, m_2, r_1). The upper set of curves are for $\tau = 2\,\mathrm{GeV}^4$ and the bottom set of curves is for $\tau = 4\,\mathrm{GeV}^4$.

all possible GSRs of gluonic and $\bar{q}q$ currents independently confirm the existence of states of mass $\sim 1\,\mathrm{GeV}$ and $\sim 1.4\,\mathrm{GeV}$ which are mixtures of gluonium and $q\bar{q}$ mesons. In particular, there is excellent agreement between the value of $r_1^{(gq)} = 0.439$ obtained from analysis of the non-diagonal NGSR and the positive solution $r_1^{(gq)} = 0.443$ in Eq. (101) resulting from the diagonal NGSRs.

Sum-Rule	m_1 (GeV)	m_2 (GeV)	r_1	r_2	s_0 (GeV^2)
diagonal: gluonic-gluonic	0.951	1.41	0.303	0.697	2.30
diagonal: $\bar{q}q$-$\bar{q}q$	0.943	1.41	0.593	0.407	2.35
non-diagonal: gluonic-$\bar{q}q$	0.869	1.39	0.439	0.561	3.00

Table 1: Analysis results from the diagonal and non-diagonal NGSRs of gluonic and $\bar{q}q$ currents in the double narrow resonance model. Central values of the QCD input parameters have been employed.

We now examine the pattern of mixing of these states as contained in the quantities r_i for the various cases. First, we note that although the fitted value of $r_1^{(gq)}$ is approximately insensitive to variations in the instanton size, the dominance of non-perturbative effects in the non-diagonal NGSR implies that there will be systematic theoretical uncertainties associated with truncation of the operator-product expansion and the single-instanton and instanton liquid approximation. An uncertainty in $r_1^{(gq)}$ of approximately 10%, at the same level as that found in the diagonal gluonic case, is therefore appropriate. Thus the value $r_1^{(gq)} = 0.439$ found from the non-diagonal case is in excellent agreement with the Eq (101) solution $r_1^{(gq)} = 0.443$ that emerges from the diagonal analyses.

If the couplings obey a single-angle mixing pattern, then one would expect $r_2^{(gg)} = \cos^2\theta = r_1^{(qq)}$. Although such a scenario could be possible given the 10% uncertainty in these quantities in Table 1, the non-diagonal case provides a more interesting test because single-angle mixing leads to

$$G_0^{(gq)}(\hat{s},\tau,s_0) = \frac{1}{\sqrt{4\pi\tau}} \sim \sin 2\theta \left[\exp\left[-\frac{(\hat{s}-m_1^2)^2}{4\tau}\right] - \exp\left[-\frac{(\hat{s}-m_2^2)^2}{4\tau}\right]\right] \ . \tag{103}$$

In this situation, the integral of the right-hand side of (103) is zero which then requires $M_0^{(gq)}(\tau,s_0) = 0$ in (68). A value of $s_0 = 4.35\,\mathrm{GeV}^2$ can be found to satisfy this constraint over the considered range $2\,\mathrm{GeV}^4 < \tau < 4\,\mathrm{GeV}^4$. However, as shown in Fig. 14 the $\hat{s}$, τ dependence of the QCD prediction $G_0^{(gq)}(\hat{s},\tau,s_0)$ is not consistent with mass scales $m_1 \approx 1\,\mathrm{GeV}$ and $m_2 \approx 1.4\,\mathrm{GeV}$. We thus conclude that the pattern of mixing for the couplings is not well-described by a single mixing angle, and hence the situation must be similar to the two-angle scenario that has been found for the η-η' system in the singlet-octet basis [45]. Implicitly this is the same result found in [5], where four independent couplings are found necessary in the study of the mixed gluonic-$q\bar{q}$ system rather than the three-parameter system of two couplings and one mixing angle.

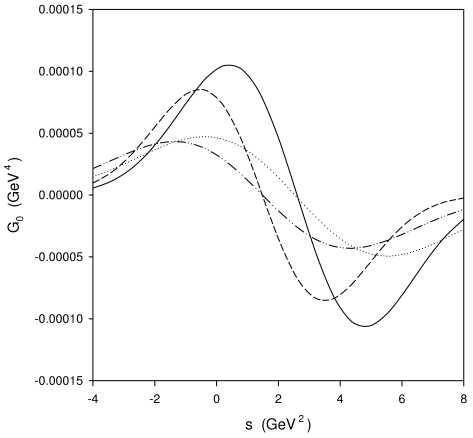

Figure 14: Comparison of the best fit of theoretical prediction for the GSR $G_0^{(gq)}(\hat{s},\tau,s_0)$ to the double narrow resonance phenomenological model for a single mixing-angle. Resonance masses $m_1 = 1\,\mathrm{GeV}$ and $m_2 = 1.4\,\mathrm{GeV}$ resulting from the analyses of the diagonal NGSRs have been employed. The optimized value of the continuum leading to $M_0 = 0$ for these resonance parameters is $s_0 = 4.35\,\mathrm{GeV}^2$. The solid and dotted curves represent $G_0^{(gq)}(\hat{s},\tau,s_0)$ and respectively correspond to $\tau = 2\,\mathrm{GeV}^4$ and $\tau = 4\,\mathrm{GeV}^4$. The dashed and dashed-dotted curves represent the single mixing-angle double resonance model and respectively correspond to $\tau = 2\,\mathrm{GeV}^4$ and $\tau = 4\,\mathrm{GeV}^4$.

In the two-angle scenario the state couplings satisfy [45]

$$f_1^{(gg)} = f_g \cos\theta_g \ , \ f_2^{(gg)} = f_g \sin\theta_g \ , \tag{104}$$

$$f_1^{(qq)} = -f_q \sin\theta_q \ , \ f_2^{(qq)} = f_q \cos\theta_q \ , \tag{105}$$

which imply that

$$r_1^{(gg)} = \cos^2\theta_g \ , \ r_2^{(gg)} = \sin^2\theta_g \tag{106}$$

$$r_1^{(qq)} = \sin^2\theta_q \ , \ r_2^{(qq)} = \cos^2\theta_q \tag{107}$$

$$r_1^{(gq)} = \frac{\sin(\theta_g - \theta_q) - \sin(\theta_g + \theta_q)}{2\sin(\theta_g - \theta_q)} \ , \ r_2^{(gq)} = \frac{\sin(\theta_g - \theta_q) + \sin(\theta_g + \theta_q)}{2\sin(\theta_g - \theta_q)} \ . \tag{108}$$

If we use the Table 1 values for the diagonal cases to determine the magnitudes of θ_g and θ_q and the non-diagonal case to determine the relative signs of the angles, then we find the central values $\theta_g = 57^\circ$ and $\theta_q = -50^\circ$.[11] This solution suggests that there is effectively a single scale for the mixing angle corresponding to a small angle solution for $\theta_g + \theta_q$. Following Ref. [12], we then define an effective mixing angle α

$$\tan^2\alpha = -\frac{\langle 0|J_g|2\rangle\,\langle 0|J_q|1\rangle}{\langle 0|J_g|1\rangle\,\langle 0|J_q|2\rangle} = -\tan\theta_g \tan\theta_q \ . \tag{109}$$

Taking into account the uncertainties in the Table 1 values and requiring that solutions to Eqs. (106)–(108) be consistent leads to $\theta_g + \theta_q = 6.5^\circ \pm 1^\circ$ and $\alpha = 54^\circ \pm 4^\circ$. Thus we find that the effective mixing angle corresponds to nearly maximal mixing ($\alpha = 45^\circ$) where each of the two states are equally coupled to the $q\bar{q}$ and gluonic currents. The deviation of our effective mixing angle from the maximal angle indicates that the heavier (1.4 GeV) state $|2\rangle$ is somewhat more gluonic in comparison to the lighter (1.0 GeV) state $|1\rangle$.

5 Discussion and Conclusions

Gaussian QCD sum-rules are able to probe hadronic spectral functions over a broad range of energy, and are thus ideally suited to exploring the possibility that mixed gluonium-$q\bar{q}$ states exist amongst the light scalar mesons. We have studied the NGSRs for all possible combinations of scalar gluonic and scalar $I = 0$ (non-strange) $q\bar{q}$ currents

[11] There remains an overall sign ambiguity in the mixing angles.

(diagonal gluonic, diagonal $q\bar{q}$, and non-diagonal $q\bar{q}$-gluonic) and find that all three cases independently predict the existence of a $\approx 1\,\text{GeV}$ state and a $\approx 1.4\,\text{GeV}$ state. This is precisely what one would expect from hadronic states that are mixtures of gluonium and quark mesons. Given the uncertainties in our mass predictions combined with the result that these predictions represent an upper bound for very broad resonances, it is not clear whether our lighter state should be interpreted as the $f_0(980)$ or σ (at the heavier end of its range [1]) and it is not clear whether the heavier state should be interpreted as the $f_0(1370)$ or the $f_0(1500)$. However, because the approximate $0.5\,\text{GeV}$ mass splitting between the states is relatively stable under QCD uncertainties, our results do suggest identifying either the lighter pair of states [σ and $f_0(1370)$] or the heavier pair [$f_0(980)$ and $f_0(1500)$] as mixed gluonium-$q\bar{q}$ states.

The non-diagonal sum-rule provides important insights into the mixing of the $q\bar{q}$ and gluonic aspects of these two states. Because of chiral suppression factors associated with the light (non-strange) quarks, perturbative effects are unable to generate any significant amount of mixing. However, the contributions of the quark condensate and instanton effects do not suffer from this chiral suppression and provide the dominant contribution to the non-diagonal correlation function, implying that mixing of gluonic and $q\bar{q}$ degrees of freedom has a non-perturbative origin. Qualitatively, this conclusion is similar to one obtained in [44] in which it was demonstrated that instantons can lead to a significant mixing between glueballs and (heavy quark) mesons in the pseudoscalar channel.

The state couplings that result from the analysis of the various GSRs also provide an additional means to examine the self-consistency of the scenario of $\approx 1\,\text{GeV}$ and $\approx 1.4\,\text{GeV}$ mixed states. In particular, the relative couplings between the states in the non-diagonal case is constrained by the relative couplings in the diagonal case. The independent prediction of these couplings from the non-diagonal NGSR is found to satisfy this constraint extremely well, providing strong evidence for the validity of the mixing scenario.

The state couplings also provide a means to study the pattern of mixing associated with the gluonic and $q\bar{q}$ currents. The resulting pattern is similar to the two-angle mixing that occurs in the η-η' system in the singlet-octet basis [45], and results in an effective mixing angle of $\alpha \approx 54^\circ$. Because this mixing angle is in the region near maximal mixing ($\alpha = 45^\circ$), there is only a slight preference for the heavier $1.4\,\text{GeV}$ state to couple to gluonic channels and a concomitantly slight preference for the lighter $1.0\,\text{GeV}$ state to couple to $q\bar{q}$ channels. Indeed, the existence of such strong mixing implies that qualitative features that would distinguish pure gluonic and $q\bar{q}$ states would be obscured for strongly-mixed states and the experimental signal of gluonium would thus be subtle.

In summary, our results provide strong evidence to support the scenario where the mixing of $q\bar{q}$ and gluonium is manifested in the scalar hadronic spectrum as a lighter state on the order of $1\,\text{GeV}$ and a heavier state on the order of $1.5\,\text{GeV}$ [2, 4, 5, 6, 9, 10, 12]. In particular, our conclusion that there exists a strong mixing between gluonium and $q\bar{q}$ states is similar to the results of Refs. [10, 12] and the heavier state's slight preference for gluonic channels has implications for the gluonium content of the $f_0(1500)$ [46].

Acknowledgements: The authors are grateful for financial support from the Natural Sciences and Engineering Research Council of Canada (NSERC). TGS dedicates this work to the memory of Victor Elias.

References

[1] W.-M. Yao et al. (Particle Data Group), J. Phys. G 33 (2006) 1.

[2] A.H. Fariborz, Phys. Rev. D74 (2006) 054030;
A.H. Fariborz, Int. J. Mod. Phys. A19 (2004) 2095.

[3] M. Albaladejo, J.A. Oller, arXiv:0801.4929v1 [hep-ph].

[4] S. Narison, G. Veneziano, Int. J. Mod. Phys. A4 (1989) 2751;
S. Narison, Nucl. Phys. B509 (1998) 312; S. Narison, Phys. Rev. D73 (2006) 114024.

[5] Tao Huang, Hong Ying Jin and Ai-lin Zhang, Phys. Rev. D59 (1998) 034026.

[6] L.S. Kisslinger, J. Gardner and C. Vanderstraeten, Phys. Lett. B410 (1997) 1.

[7] D. Harnett, T.G. Steele, Nucl.Phys. A695 (2001) 205.

[8] G. Orlandini, T.G. Steele, D. Harnett, Nucl.Phys. A686 (2001) 261.

[9] T.G. Steele, D. Harnett, G. Orlandini, AIP Conf. Proc. 688 (2004) 128 [arXiv:hep-ph/0308074].

[10] P. Minkowski, W. Ochs, Eur. Phys. J. C9 (1999) 283;
Peter Minkowski, Wolfgang Ochs, arXiv:hep-ph/0209225.

[11] C.J. Morningstar, M. Peardon, Phys. Rev. D60 (1999) 034509;
A. Vaccarino, D. Weingarten, Phys. Rev. D60 (1999) 114501;
Y. Chen *et al*, Phys. Rev. D73 (2006) 014516.

[12] UKQCD Collaboration: A. Hart, C. McNeile, C. Michael, J. Pickavance, Phys. Rev. D74 (2006) 114504.

[13] V.A. Novikov, M.A. Shifman, A.I. Vainshtein and V.I. Zakharov, Nucl. Phys. B191 (1981) 301.

[14] S. Narison, N. Pak, N. Paver, Phys. Lett. B147 (1984) 162.

[15] R.A. Bertlmann, G. Launer, E. de Rafael, Nucl. Phys. B250 (1985) 61.

[16] P. Pascual and R. Tarrach, Phys. Lett. B113 (1982) 495.

[17] N.K. Nielsen, Nucl. Phys. B120 (1977) 212;
J.C. Collins, A. Duncan, S.D. Joglekar, Phys. Rev. D16 (1977) 438.

[18] R. Tarrach, Nucl. Phys. B196 (1982) 45.

[19] E.V. Shuryak, Nucl. Phys. B203 (1982) 93.

[20] H. Forkel, Phys. Rev. D64 (2001) 034015;
D. Harnett, T.G. Steele, V. Elias, Nucl. Phys. A686 (2001) 393.

[21] K.G. Chetyrkin, B.A. Kneihl and M. Steinhauser, Nucl. Phys. B510 (1998) 61;
A.L. Kataev, N.V. Krasnikov, A.A. Pivovarov, Nucl. Phys. B198 (1982) 508, Erratum-ibid B490 (1997) 505.

[22] E. Bagan and T.G. Steele, Phys. Lett. B234 (1990) 135;
D. Harnett, T.G. Steele, JHEP 0412 (2004) 037.

[23] V.A. Novikov, M.A. Shifman, A.I. Vainshtein and V.I. Zakharov, Nucl. Phys. B165 (1980) 67.

[24] A. Belavin, A. Polyakov, A. Schwartz and Y. Tyupkin, Phys. Lett. B59 (1975) 85;
G. 't Hooft, Phys. Rev. D14 (1976) 3432.

[25] T. Schäefer and E.V. Shuryak, Phys. Rev. Lett. 75 (1995) 1707.

[26] B.V. Geshkenbein and B.L. Ioffe, Nucl. Phys. B166 (1980) 340;
B.L. Ioffe and A.V. Samsonov, Phys. of Atom. Nucl. 63 (2000) 1527.

[27] M. Abramowitz and I.E. Stegun, *Mathematical Functions with Formulas, Graphs, and Mathematical Tables* (National Bureau of Standards Applied Mathematics Series, Washington) 1972.

[28] K.G. Chetyrkin, Phys. Lett. B390 (1997) 309;
S.G. Gorishny, A.L. Kataev, S.A. Larin, L.R. Surguladze, Phys. Rev. D43 (1991) 1633 and Mod. Phys. Lett. A5 (1990) 2703.

[29] M.A. Shifman, A.I. Vainshtein and V.I. Zakharov, Nucl. Phys. B147 (1979) 385, 448.

[30] D. Binosi and L. Theußl, Comp. Phys. Comm. 161 (2004) 76.

[31] S. Narison, Phys. Rep. 84 (1982) 263.

[32] E. Bagan, M.R. Ahmady, V. Elias, T.G. Steele, Z. Phys. C61 (1994) 157.

[33] E. Bagan, J.I. Latorre, P. Pascual, Z. Phys. C32 (1986) 43.

[34] L.S. Kisslinger, M.B. Johnson, Phys. Lett. B523 (2001) 127.

[35] S. Narison, Z. Phys. C26 (1984) 209;
H. Forkel, Phys. Rev. D71 (2005) 054008.

[36] E. Bagan and T.G. Steele, Phys. Lett. B243 (1990) 413.

[37] J. Bordes, V. Gimènez and J.A. Peñarrocha, Phys. Lett. B223 (1989) 251;
J.L. Liu and D. Liu, J. Phys. G19 (1993) 373.

[38] M.A. Shifman, Z. Phys. C9 (1981) 347.

[39] C.A. Dominguez and N. Paver, Z. Phys. C31 (1986) 591.

[40] V. Elias, A.H. Fariborz, Fang Shi, T.G. Steele, Nucl. Phys. A633 (1998) 279.

[41] S. Narison, Nucl. Phys. B (Proc. Supp.) 54A (1997) 238.

[42] E. Bagan, J.I. Latorre, P.Pascual and T. Tarrach, Nucl. Phys. B254 (1985) 555.

[43] V. Giménez, J. Bordes, J. Peñarrocha, Nucl. Phys. B357 (1991) 3;
C.A. Dominguez, J. Sola, Z. Phys. C40 (1988) 63.

[44] N. Kochelev and Dong-Pil Min, Phys. Rev. D72 (2005) 097502.

[45] Th. Feldmann, P. Kroll, B. Stech, Phys. Rev. D58 (1998) 114006 and Phys. Lett. B449 (1999) 339.

[46] C. Amsler and F.E. Close, Phys. Rev. D53 (1996) 295;
L. Burakovsky and P.R. Page, Phys. Rev. D59 (1999) 014022;
F.E. Close, Qiang Zhao, Phys. Rev. D71 (2005) 094022.